2D Nanomaterials

International Edition: DOI: 10.1002/anie.201509933
German Edition: DOI: 10.1002/ange.201509933

Solution-Processed Two-Dimensional MoS_2 Nanosheets: Preparation, Hybridization, and Applications

*Xiao Zhang+, Zhuangchai Lai+, Chaoliang Tan, and Hua Zhang**

Keywords:
MoS_2 · nanosheets · solution processes · 2D nanomaterials

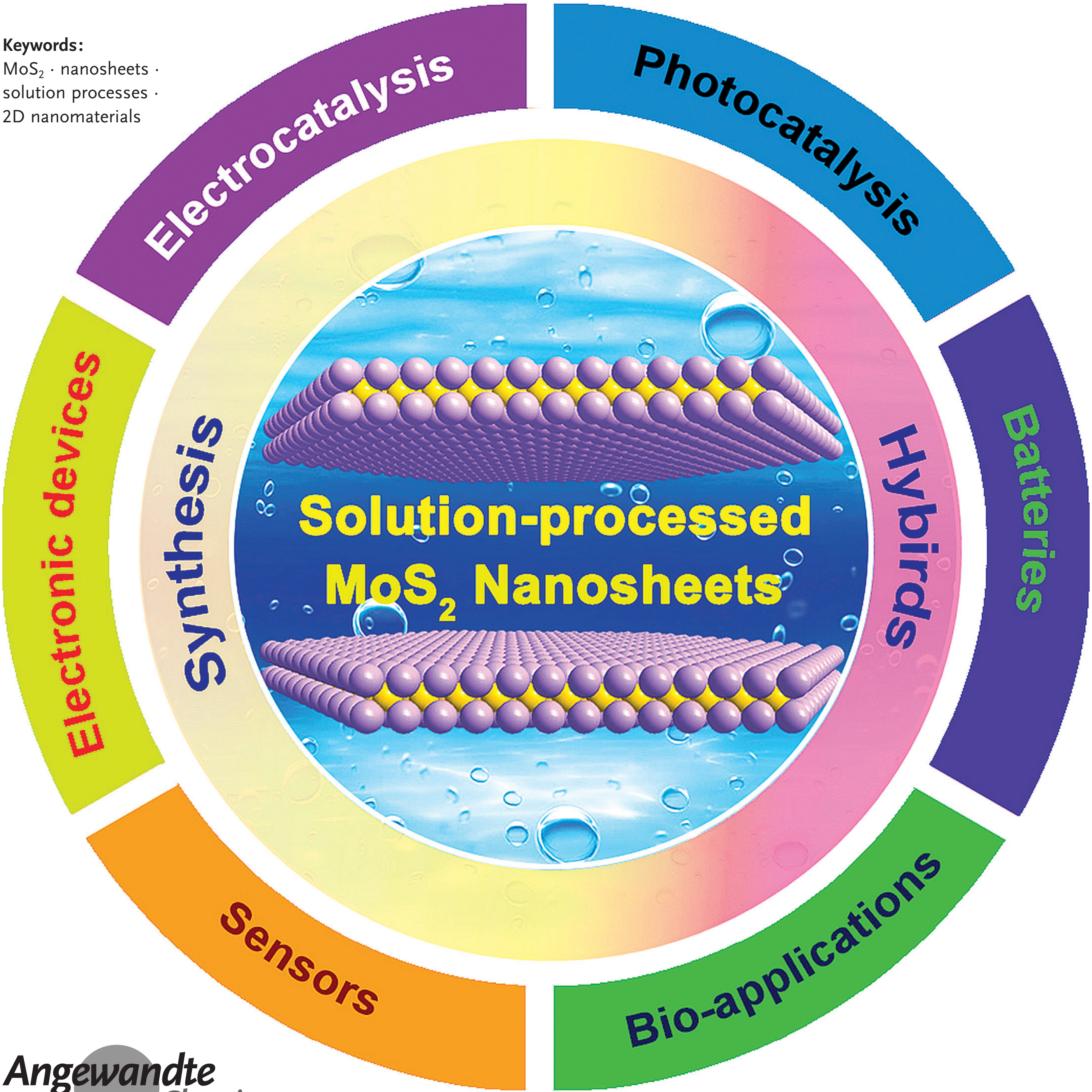

© 2016 Wiley-VCH Verlag GmbH & Co. KGaA, Weinheim

As one member of the emerging class of ultrathin two-dimensional (2D) transition-metal dichalcogenide (TMD) nanomaterials, the ultrathin MoS_2 nanosheet has attracted increasing research interest as a result of its unique structure and fascinating properties. Solution-phase methods are promising for the scalable production, functionalization, hybridization of MoS_2 nanosheets, thus enabling the widespread exploration of MoS_2-based nanomaterials for various promising applications. In this Review, an overview of the recent progress of solution-processed MoS_2 nanosheets is presented, with the emphasis on their synthetic strategies, functionalization, hybridization, properties, and applications. Finally, the challenges and opportunities in this research area will be proposed.

From the Contents

1. Introduction

The successful exploration of graphene has recently evoked enormous research enthusiasm on the graphene-like two-dimensional (2D) layered materials.[1] As a typical example, transition-metal dichalcogenides (TMDs), especially the ones with atomic thickness, have been emerging as a new class of nanomaterials for fundamental studies and promising applications owing to their intriguing properties.[2] TMDs are the MX_2-type compounds, where M is a transition-metal element and X a chalcogen, that is, S, Se, or Te. TMDs can be semiconductors, metals, or insulators,[2d,f] exhibiting diverse properties. Among TMDs, MoS_2 is one of the most promising semiconductors because of its inherent and thickness-dependent band gap as well as its abundance in nature as molybdenite.[3] Moreover, bulk MoS_2 crystals can be exfoliated to single- or few-layer nanosheets, exhibiting unusual physical and electronic properties.[2d,3i,4] For example, a transition from indirect band gap to direct band gap occurs as the thickness of MoS_2 decreased to monolayer. Specifically, bulk MoS_2 is a semiconductor with narrow band gap of about 1.3 eV, while the isolated MoS_2 monolayer possesses a large band gap of 1.8–1.9 eV. Driven by these unique properties and state-of-the-art synthetic methods, single- and few-layered MoS_2 nanosheets have been extensively investigated for a wide range of applications in electronics/optoelectronics,[3a,f,5] sensors[6] and energy-storage and conversion devices.[7]

Owing to the layered structure similar to graphene, most of the methods used for isolation or preparation of graphene are also effective for MoS_2 nanosheets. For example, the micromechanical cleavage using scotch-tape is a traditional and straightforward way for preparation of high-quality pristine graphene,[8] which can also be used to prepare MoS_2 nanosheets.[3a,b,g,5a,c,6c,9] However, it lacks sufficient scalability for large-scale production, and the size and thickness of the resultant MoS_2 nanosheets is difficult to control. Chemical vapor deposition (CVD) is an effective method for growth of high-quality MoS_2 sheets with controllable size and thickness,[10] but the rigid experimental requirements, such as high temperature, high vacuum, and specific substrates, limit the widely practical applications of MoS_2 sheets. Aiming to the scalable production of MoS_2 nanosheets in high yield and engineering their chemical and physical properties to achieve improved performance in applications, solution-based methods hold particular promise.[2b,e,6a,11] Compared to other methods, the advantages of solution-based methods for preparation of MoS_2 nanosheets include: 1) utilization of low-cost precursors, such as metal salts or earth-abundant MoS_2 powders; 2) scalability for large-scale production of MoS_2 nanosheets with high throughput; 3) solution-processed nanosheets can be easily sorted and separated, resulting in nanosheets with desirable size and thickness; 4) the versatile chemical properties and solubility provide a rich platform for chemical functionalization and hybridization with other materials in solution; 5) MoS_2 nanosheets in solution can be conveniently transferred onto any substrates in a simple process.

In this Review, we summarize the state-of-art studies of solution-processed MoS_2-based materials, aiming to give an overview of this emerging material and discuss the challenges and opportunities in this promising research area. Not only the preparation, characterization, and hybridization, but also the applications of solution-processed MoS_2 nanosheets will be discussed. First, the preparation methods for MoS_2 nanosheets in solution will be classified and highlighted. Then, a detailed description of MoS_2 nanosheet-based hybrids will be presented, and the potential applications will be summarized. Finally, our personal insights on the challenges and future prospects for this research area will be provided.

[*] X. Zhang,[+] Z. C. Lai,[+] C. L. Tan, Prof. H. Zhang
Center for Programmable Materials, School of Materials Science and Engineering, Nanyang Technological University
50 Nanyang Avenue, Singapore 639798 (Singapore)
E-mail: hzhang@ntu.edu.sg
Homepage: http://www.ntu.edu.sg/home/hzhang/
X. Zhang[+]
Energy Research Institute @ NTU (ERI@N), Interdisciplinary Graduate School, Nanyang Technological University
50 Nanyang Drive, Singapore 637553 (Singapore)
[+] These authors contributed equally to this work.

 © 2016 Wiley-VCH Verlag GmbH & Co. KGaA, Weinheim

2. Synthesis and Characterization of MoS_2 Nanosheets

Solution-based techniques for preparation of MoS_2 nanosheets can be classified into two categories, that is, liquid-phase exfoliation methods (top-down method)[2e,6a,11a] and wet chemical synthesis methods (bottom-up method).[12] The liquid-phase exfoliation is described as a dispersion/exfoliation method, and the basic idea is to weaken the interaction of adjacent layers of MoS_2. To achieve this goal, dispersion chemicals, such as reaction reagents, solvents, or surfactants, are necessary, which greatly determine the exfoliation yield and quality of MoS_2 nanosheets.[2e,6a,11a] The affinity between host materials and dispersion chemicals weakens the interlayer interactions of MoS_2, and the subsequent sonication leads to the isolation of sheets. In contrast, wet chemical method is a typical bottom-up process, which relies on the chemical reaction of metal-salts as precursors to prepare MoS_2 nanosheets.[12,13]

2.1. Solvent-Assisted Exfoliation Methods

Solvent-assisted exfoliation method, that is, immersion of layered bulk materials into organic solvents and then sonication, is one of the most straightforward methods for exfoliation of layered materials.[2e,11a,14] This method has been well developed for exfoliation of graphite into graphene.[14a,b] It has been demonstrated that the dispersion solvents play a key role in determining the exfoliation yield. When a solid surface is immersed in a liquid medium, the energetic cost of exfoliation becomes minimal when the surface tension of solvent matches that of layered materials. Importantly, the suitable solvent guarantees the stable dispersion of nanosheets against their re-stacking and aggregation. In 2011, Coleman and co-workers exfoliated single- and few-layered MoS_2 nanosheets by sonication of bulk MoS_2 powder in organic solvents.[11a] Experimental results derived from their exfoliation studies suggested that the effective solvent should have certain surface tension close to 40 $mJ\,m^{-2}$, and 1-methyl-2-pyrrolidone (NMP) was the most effective solvent for exfoliation of MoS_2. The lateral size of the obtained MoS_2 nanosheets is in the range of 50 to 1000 nm, and the concentration is around 0.3 $mg\,mL^{-1}$ in NMP. Moreover, it has been demonstrated that this process is also suitable for exfoliation of other TMD materials, such as TiS_2, TaS_2, $MoSe_2$. Later, the same group systematically investigated the experimental parameters, for example, starting mass, sonication power, sonication time, and centrifugation conditions, on the exfoliation of MoS_2 in NMP.[15] It was found that the concentration of MoS_2 nanosheets scales linearly with the starting MoS_2 mass and can be maximized for an initial MoS_2 concentration of 100 $mg\,mL^{-1}$. Furthermore, by controlling the centrifugation process, large-size flakes can be obtained with mean flake length of approximately 2 μm and maximum length of 4–5 μm.[15] Most importantly, the concentration of exfoliated MoS_2 nanosheets is increased to 40 $mg\,mL^{-1}$ by increasing the sonication time to 200 h. However, the nanosheets produced by long-time sonication usually exhibit small lateral size and broad size distribution. Moreover, the

Xiao Zhang received his B.S. and M.S. degrees from Harbin Engineering University in 2010 and 2013, respectively. Then, he moved to the Interdisciplinary Graduate School of Nanyang Technological University in Singapore in 2013 as a PhD student under the supervision of Prof. Hua Zhang. His research interests are the synthesis and applications of novel two-dimensional nanomaterials.

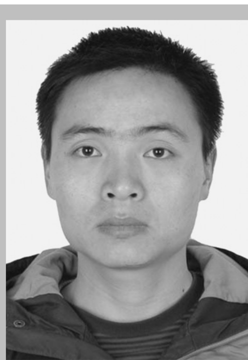

Chaoliang Tan received his B.Eng. and M.Eng. degrees from Hunan University of Science and Technology (2009) and South China Normal University (2012). Currently, he is a PhD student at the School of Materials Science and Engineering of the Nanyang Technological University in Singapore under the supervision of Prof. Hua Zhang. His research interests focus on the synthesis, assembly, and applications of two-dimensional nanosheets and their composites.

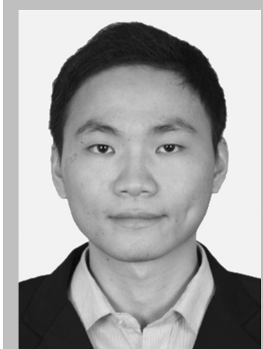

Zhuangchai Lai received his B.S. degree in Materials Chemistry from Sun Yat-sen University in 2009 and his M.Eng. degree in Industrial Catalysis from South China University of Technology in 2012. He then worked as a research assistant with Prof. Feng Peng before moving to the School of Materials Science and Engineering at the Nanyang Technological University in Singapore in 2014 to pursue his PhD degree with Prof. Hua Zhang. His current research interests include the synthesis and applications of two-dimensional nanomaterials and their composites.

Hua Zhang obtained his B.S. (1992) and M.S. (1995) degrees at Nanjing University, and completed his Ph.D. with Prof. Zhongfan Liu at Peking University in 1998. As a Postdoctoral Fellow, he joined Prof. Frans C. De Schryver's group at Katholieke Universiteit Leuven (Belgium) in 1999, and then moved to Prof. Chad A. Mirkin's group at Northwestern University in 2001. After he worked at NanoInk Inc. (USA) and Institute of Bioengineering and Nanotechnology (Singapore), he joined Nanyang Technological University in 2006. His current research interests focus on the synthesis of ultrathin two-dimensional nanomaterials, semiconducting nanomaterials, and complex heterostructures.

© 2016 Wiley-VCH Verlag GmbH & Co. KGaA, Weinheim

problems of using NMP, such as its toxicity and the difficult removal of nanosheets from it, are detrimental for some specific applications.[14b,16]

To overcome the limitations of NMP, development of other exfoliation methods using aqueous solution or volatile solvent is required. Recently, the Hansen solubility parameter (HSP) theory, a typical semi-empirical correlation, was used to explain the dissolution-behavior-related parameters, such as the dispersive, polar, and hydrogen-bonding interactions of solvent and materials.[11a,17] Based on the HSP theory, a series of co-solvents were developed for the exfoliation of MoS_2. As a typical example, Zhang and co-workers demonstrated that the mixture of water and ethanol was effective for exfoliating and dispersing MoS_2 nanosheets.[18] It is noteworthy that water and ethonol individually are inefficient in exfoliating owing to the large surface-energy difference from the bulk MoS_2. However, mixing of solvents changed the solubility parameters, resulting in the most effective solubility of MoS_2 nanosheets in the mixture of 45 vol% ethanol in water, which was the optimal condition for isolation of MoS_2 nanosheets. The highest concentration of MoS_2 nanosheets is estimated to be 0.018 ± 0.003 mg mL^{-1}. Significantly, the non-toxic water and ethanol are both commonly used solvents that can be easily removed. In addition, the volatile mixture of chloroform and acetonitrile was also used to prepare few-layer MoS_2 nanosheets with the concentration of 0.4 mg mL^{-1}.[19]

To predict the optimal co-solvent concentration for the exfoliation of MoS_2 in the mixture of water and alcohol, Duan and co-workers designed an effective method by directly determining the liquid–solid interfacial energy though the contact angle.[20] Four kinds of alcohol, that is, methanol, ethanol, isopropanol, and *tert*-butyl alcohol, were mixed with water. It was shown that the co-solvent concentration was critical for the exfoliation yield which could be greatly increased by addition of 10–30 wt% *tert*-butyl alcohol or isopropanol to water. Importantly, the molecular length of the co-solvent also played a crucial role for the exfoliation. The yield increased by using larger co-solvent molecules, that is, more -CH_3 groups, and followed the trend methanol < ethanol < isopropanol < *tert*-butyl alcohol. Compared to using the HSP theory, this method is facile and it is not necessary to make any assumption about the solubility parameters of materials.

Very recently, Lu and co-workers demonstrated that the mixture of H_2O_2 and NMP could be a good solvent for spontaneous exfoliation of MoS_2 in mild conditions.[21] The yield of MoS_2 nanosheets is over 60 wt%. Interestingly, the H_2O_2 cannot only induce the spontaneous exfoliation of MoS_2 in NMP, but also lead to concurrent dissolution of MoS_2 nanosheets. By finely tuning the concentration of H_2O_2, the morphology of the MoS_2 samples produced changed from nanosheets to porous nanosheets, and finally nanodots, which were obtained in a high concentration of H_2O_2. Although the mixing of H_2O_2 in NMP can enhance the exfoliation yield of MoS_2 nanosheets, this method is difficult to operate and H_2O_2 may cause unexpected oxidation of MoS_2 and introduce some defects in the MoS_2 nanosheets.

2.2. Surfactant/Polymer-Assisted Exfoliation Methods

Liquid-phase exfoliation, assisted by organic compounds, is another feasible route for the isolation of MoS_2 nanosheets.[5d,22] Small organic molecules, surfactants, or polymers, especially those who have a high adsorption energy on the basal plane of MoS_2 nanosheets, can greatly promote MoS_2 exfoliation. As a representative example, Coleman and co-workers demonstrated the preparation of MoS_2 nanosheets by using 1.5 mg mL^{-1} sodium cholate in aqueous solution.[22a] The sodium cholate was used as the ionic surfactant to assist the exfoliation and stabilization of MoS_2 nanosheets, forming sodium cholate-coated MoS_2 nanosheets. The surface potential was measured to be −40 mV, which was stable against the change of pH. Additionally, the dispersion is stable in aqueous solution and can be easily hybridized with carbon nanotubes (CNTs) and graphene. Similarly, Huang and co-workers developed an alkylamine-assisted liquid sonication method for the exfoliation of MoS_2 nanosheets.[22b] In their experiment, several amines with different alkyl chains, for example, butylamine, octylamie, and dodecylamine, were tested. It was found that butylamine in NMP is efficient and can dramatically increase the yield. Importantly, the MoS_2 nanosheets produced are stable in a series of polar and nonpolar organic solvents for months. Alternatively, Guardia and co-workers demonstrated the exfoliation of MoS_2 nanosheets by using non-ionic surfactants as stabilization and dispersing agents.[22c] Nine non-ionic surfactants were used, that is, polyoxyethylene sorbitan monooleate (Tween 80), polyoxyethylene sorbitan trioleate (Tween 85), polyvinylpyrrolidone (PVP), polyoxyethylene(4)dodecyl ether (Brij 30), polyoxyethylene(100)octadecyl ether (Brij 700), polyoxyethyleneoctyl(9-10)phenylether (Triton X-100), gum Arabic from acacia tree, Pluronic P-123, and *n*-dodecyl β-D-maltoside (DBDM). Meanwhile, the anionic surfactant sodium cholate (SC) was used as reference. Among these surfactants, P-123 offered the highest efficiency for the exfoliation of MoS_2 nanosheets. Similarly, our group demonstrated that PVP can largely improve the exfoliation and dispersion of MoS_2 nanosheets from its bulk material in ethanol.[5d] However, since PVP has excellent solubility and wetting properties, it easily adsorbed on the MoS_2 surface, forming PVP-coated MoS_2 hybrid nanosheets. Very recently, Han and co-workers reported the exfoliation of MoS_2 nanosheets in water by using bovine serum albumin (BSA).[23] The BSA is used as the exfoliating agent, and also acts as a strong stabilizing agent against the aggregation of MoS_2 nanosheets. Similar to the PVP-assisted exfoliation process, BSA can also adsorb on MoS_2 layers. The obtained composites exhibit good biocompatibility and show higher binding capacity to pesticides.

2.3. Ion-Intercalation/Exfoliation Methods

Inorganic ions are effective intercalators to improve the exfoliation efficiency of layered materials. The studies on graphene suggest that ion intercalation occurs in highly anisotropic layered structures with weak interlayer interac-

© 2016 Wiley-VCH Verlag GmbH & Co. KGaA, Weinheim

tions.[24] Because MoS_2 has a small interlayer space, approximately 6.5 Å, only Lewis bases and alkali-metal ions with small radii are able to enter the interlayer space of bulk MoS_2.[24] Typically, Li-ion intercalation is one of the most popular and efficient ways for exfoliating layered materials, and has been used for the exfoliation of MoS_2 nanosheets. Usually, this method requires three steps: 1) intercalation of Li^+ ions into the interlayer space of bulk MoS_2; 2) immersion of the Li-intercalated compounds in water; and 3) sonication of the compounds. It is noteworthy that the Li-ion intercalation of MoS_2 could lead to its structure transformation from the hexagonal (2H) phase to octahedral (1T) phase.[2f,3h,6a,7a,11b] The 2H-MoS_2 is semi-conductive whereas the 1T-MoS_2 is metallic.[11b] Although Chhowalla and co-workers reported the preparation of single-layer MoS_2 by using *n*-butyllithium as the intercalation source,[3h,11b] forcing conditions, such as elevated temperature and long reaction time (3 days) were required, and the amount of intercalated Li^+ ions cannot be controlled in this process. Recently, Loh and co-workers prepared high-quality single-layer MoS_2 nanosheets by using two-step expansion and intercalation process.[25] The first expansion step was carried out by treating bulk MoS_2 with hydrazine (N_2H_4) in a hydrothermal reaction. It was found that the volume of MoS_2 crystals expanded by more than 100 times after the decomposition of intercalated N_2H_4 molecules. Afterwards, the expanded MoS_2 crystals were intercalated by metal naphthalenide (metal includes Li, Na, and K) and then sonicated in water to induce the exfoliation. The high-yield (90%) production of single-layer MoS_2 nanosheets with size up to 400 μm^2 after purification was achieved. However, despite the high efficiency and good dispersity of the exfoliated MoS_2 nanosheets, the process is dangerous because the intercalated compounds might self-heat, self-ignite, or self-explode in air.

Compared to the aforementioned methods, our recently developed method, that is, the electrochemical lithiation-interclation process, shows some advantages.[6a] Briefly, the experiment is performed in a battery test system with a MoS_2-containing cathode and lithium-foil anode (Figure 1 a). During the galvanic discharge process in the cell, Li^+ ions were intercalated into the layered MoS_2. Subsequent ultrasonication of Li-intercalated compounds (e.g. Li_xMoS_2, where x is the number of Li atoms in Li_xMoS_2) in water yields a large quantity of well-dispersed single-layer MoS_2 nanosheets (Figure 1 b,c). The resulting single-layer MoS_2 nanosheets were prepared in yields as high as 92% (after purification). The greatest advantage of this method is that the amount of intercalated Li^+ ions can be precisely monitored and controlled by setting the cut-off voltage at different stages. Note that the exfoliated MoS_2 nanosheets have two kinds of structural phases, which can be tuned by controlling the discharge process. Recently, Wang and co-workers gave a detailed description about the structural evolution of MoS_2 by controlling the intercalation of Na^+ ions through a similar electrochemical method.[26] Because the content of intercalated Na^+ ions is directly proportional to the discharge time, the phase transformation from semiconducting 2H-MoS_2 to metallic 1T-MoS_2 was easily controlled by tuning the cut-off discharge potential or time in a galvanostatic mode.

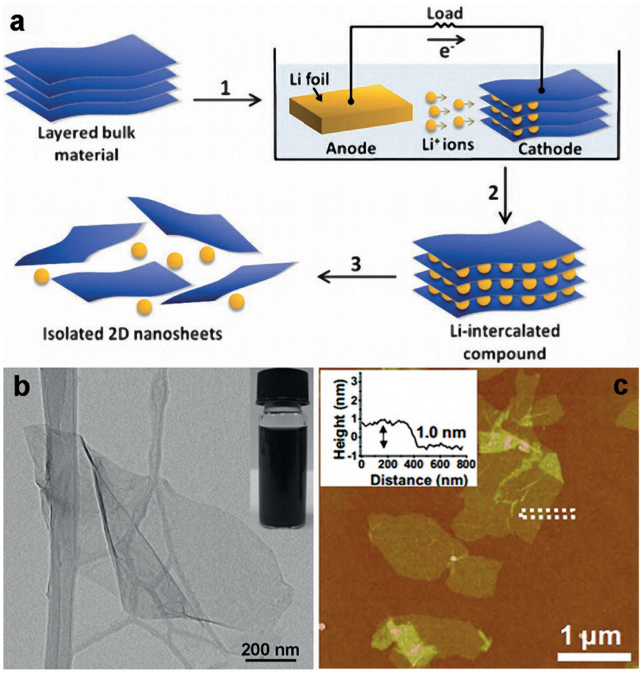

Figure 1. a) Schematic illustration of electrochemical lithiation and exfoliation process for the fabrication of 2D nanosheets from layered bulk crystals. b) TEM image of a typical MoS_2 nanosheet. Inset: Photograph of the MoS_2 solution. c) AFM image of MoS_2 nanosheets deposited on Si/SiO_2 substrates. Reproduced with permission from Ref. [6a]. Copyright 2011, John Wiley & Sons, Inc.

Interestingly, it was suggested that 1.5 Na^+ ions per formula unit of MoS_2 (Na_xMoS_2, $x=1.5$) was a critical point for the reversibility of the structure evolution of MoS_2. If the intercalated Na^+ ion is less than 1.5 per formula (i.e. $x<1.5$), the structure of MoS_2 can be partially recovered to MoS_2, while $x>1.5$ would induce the irreversible decomposition of Na_xMoS_2 into Na_xS and metallic Mo. Furthermore, Cui and co-workers also demonstrated that the oxidation state of Mo, the transition of 2H to 1T as well as the layer spacing of MoS_2 could be continuously tuned by the electrochemical intercalation of Li^+ ions in a vertically aligned MoS_2 films.[27] It is known that 1T-MoS_2 can revert back to 2H-MoS_2 upon annealing at high temperatures of above 300 °C.[3h] However, the process requires the drying of the MoS_2 nanosheets, limiting the further processability of the MoS_2 nanosheets. Very recently, Dravid and co-workers demonstrated the controllable recovery of the semiconducting properties of Li-treated MoS_2 nanosheets directly in solution.[28] Briefly, the exfoliated MoS_2 nanosheets were first transferred from water to organic solvents, such as *o*-dichlorobenzene (ODCB), via the biphasic reaction using oleylamine as the cationic amphiphile reagent. The recovery of semiconducting properties of MoS_2 nanosheets was then finished by thermal-annealing of the nanosheets in inert, high-boiling-point organic solvents, such as octadecene (boiling point of 315 °C), and *o*-dichlorobenzene (ODCB) (with boiling point of 180 °C). Importantly, the treated MoS_2 nanosheets still can be transferred and assembled into free-standing films and patterns.

 © 2016 Wiley-VCH Verlag GmbH & Co. KGaA, Weinheim

In addition to the ion intercalation, inorganic salt-assisted exfoliation is another efficient way for exfoliation of MoS_2 nanosheets.[29] The intercalated salt ions can greatly decrease the interaction between layers when the solution becomes supersaturated after the evaporation of water, thus improving the exfoliation efficiency of nanosheets. Moreover, the salt ions can be used as electrostatic stabilizers adsorbed on the surface of exfoliated nanosheets, thus enhancing the stability of exfoliated nanosheet suspension. For example, Zheng and co-workers prepared single- and few-layer MoS_2 nanosheets with the aid of non-toxic $CuCl_2$ and NaCl.[29a] Importantly, the MoS_2 nanosheets obtained preserved their single crystallinity, which is critical for electro-optical applications.

Choi and co-workers reported a similar technique for the exfoliation of MoS_2 in NMP by using MOH (M = Li, Na, and K) as intercalators.[29b] NMP has a sufficiently high dielectric strength for MoS_2, which promotes the incorporation of Li^+ (or Na^+, K^+) and OH^- ions into the interlayer space of MoS_2, thus improving the dispersity of MoS_2 nanosheets. Despite the enhanced exfoliation efficiency, most exfoliated MoS_2 nanosheets showed thickness of around 1–9 nm, that is, 1–9 layers.

2.4. Other Sonication Methods

To improve the exfoliation efficiency, external force can also be used to prepare MoS_2 nanosheets. Typically, mechanical grinding, generating shear force, was used to detach the MoS_2 layers from the bulk materials, and thus promoting the exfoliation yield of MoS_2 nanosheets.[30] For example, Wong and co-workers prepared high-concentration aqueous solutions of MoS_2 nanosheets by a combination of grinding and sonication techniques.[30] Briefly, bulk MoS_2 powder was first ground in NMP. After separating from NMP through centrifugation, MoS_2 were then sonicated in the ethanol/water solution (v:v = 45:55). The concentration of the as-obtained MoS_2 nanosheet suspension in ethanol/water solution significantly increased to $26.7 \pm 0.7\ \mathrm{mg\,mL^{-1}}$. Similarly, the NMP solution[31] and a mixture of sodium dodecyl sulfate (SDS) and water[32] have also been used for exfoliation of MoS_2 by grinding-assisted sonication. Very recently, Kalantar-zadeh and co-workers systematically investigated the solvent effect on the exfoliation of MoS_2 nanosheets by using grinding-assisted exfoliation, highlighting the importance of the grinding step and the choice of solvent.[33] Typically, several kinds of solvents, such as acetone, acetonitrile, benzene, cyclohexane, hexane, isopropanol, methanol, and toluene, are used in the grinding step, which have lower boiling points and surface tension energies than NMP. After grinding, the sample was re-dispersed in ethanol prior to sonication and centrifugation. It was found that the solvent during grinding plays a critical role in determining the exfoliation yield as well as the flake sizes and thickness. Interestingly, only four grinding solvents, that is, NMP, hexane, cyclohexane, and acetonitrile, led to the exfoliation of MoS_2. Specifically, by using NMP as the grinding solvent, MoS_2 flakes with lateral size of 20–200 nm and thickness of 1.5–3.5 nm were obtained in the highest quality. However, Raman spectroscopy showed that NMP is difficult to remove, and it can remain on the surface of MoS_2 nanosheets even after sonication in ethanol. It means that NMP is a persistent residue adsorbed on the exfoliated nanosheets and may affect the properties of MoS_2 nanosheets.

Very recently, Wei and co-workers demonstrated that the "quenching cracks" induced by liquid N_2 could greatly enhance the exfoliation efficiency of MoS_2 nanosheets, since the quenching cracks induced by instant cooling might break the van der Waals force between the adjacent layers of MoS_2.[34] However, care must be taken when using this method because liquid N_2 must be handled with caution.

Alternatively, electrochemical exfoliation using a two-electrode cell is another way to exfoliate MoS_2 nanosheets. For example, Lee and co-workers reported the electrochemical exfoliation of MoS_2 by using a bulk MoS_2 crystal as a working electrode, Pt wire as the counter electrode, and Na_2SO_4 solution as electrolyte.[35] A direct current (DC) bias was applied to the two-electrode system for electrochemical exfoliation. The yield of MoS_2 nanosheets was about 5–9% and the concentration was in the range of 0.007–$0.014\ \mathrm{mg\,mL^{-1}}$. Importantly, the lateral size of exfoliated MoS_2 nanosheets was quite large at 5–50 μm. However, most of the synthesized nanosheets were multi-layers instead of well-dispersed single-layer nanosheets. Moreover, the exfoliated MoS_2 nanosheets undergo a small degree of oxidation during the electrochemical exfoliation.

2.5. Wet Chemical Synthesis Methods

Wet chemical synthetic methods, that is, bottom-up methods, have been explored to synthesize MoS_2 nanosheets with desired size and thickness. Two typical approaches for the preparation of MoS_2 nanosheets are hydrothermal and hot-injection methods using metal salts as precursors.[12,13]

The hydrothermal method is attractive because of its simplicity and wide applicability.[1g,13a,36] Usually, the hydrothermal process is conducted in a sealed autoclave at elevated temperature and high vapor pressure. As a typical example, Rao and co-workers synthesized MoS_2 nanosheets by the hydrothermal treatment of MoO_3 and KSCN (as the sulfur source) in water at 453 K.[12] The MoS_2 nanosheets with few-layer thicknesses and layer separation of 0.65–0.7 nm were obtained. Recently, Xie and co-workers demonstrated the preparation of defect-rich MoS_2 nanosheets using the hydrothermal method. During the reaction, thiourea was used to reduce Mo(VI) to Mo(IV), and also acted as an additive to stabilize the ultrathin MoS_2 nanosheets.[37] Note that the hydrothermal process occurs at high temperature and pressure, and the obtained MoS_2 nanosheets normally aggregate to form structures such as nanoflowers[38] and nanotubes.[13a] For example, very recently, Wang and co-workers demonstrated that three-dimensional (3D) tubular architectures of MoS_2 can be obtained through hydrothermal reaction in a mixed solution.[13a] Briefly, the process was conducted in the mixture of ethanol and octylamine at 200–220 °C by using ammonium molybdate ($(NH_4)_2MoS_4$) and sulfur powder as precursors. The 3D tubes formed by the spontaneous self-assembly of MoS_2 nanosheets, exhibited high specific surface

 © 2016 Wiley-VCH Verlag GmbH & Co. KGaA, Weinheim

area and mesoporous structure. Since the ultrathin 2D nanosheets are easy to wrinkle, it is difficult to obtain well-dispersed single-layer MoS_2 nanosheets by using hydrothermal method.

Alternatively, the hot-injection method was developed for preparation of MoS_2 nanosheets. This reaction is usually carried out in a high-boiling-point organic medium where the effective nucleation and growth process occurs. Specifically, organic ligands are necessary, which are used to control the size and morphology of synthesized MoS_2 nanosheets as well as improve their dispersibility. For example, Altavilla and co-workers reported the synthesis of free-standing MoS_2 nanosheets by high-temperature (360 °C) decomposition of single-source precursors, that is, ammonium tetrathiomolybdate, in the presence of oleylamine.[13b] Briefly, the precursor, that is, ammonium tetrathiomolybdate, was stirred in oleylamine under N_2 flow at 100 °C for 15 min. Then the mixture was heated up to 360 °C. Importantly, the thickness of the MoS_2 nanosheets obtained can be tuned from single layer to few layers as the reaction time increasing from 30 to 90 min. Note that the MoS_2 nanosheets were coated by oleylamine which stabilized their suspension and prevented their aggregation and oxidation. Similarly, Rao and co-workers demonstrated the synthesis of MoS_2 nanosheets by using molybdic acid and excess thiourea at 773 K under N_2 atmosphere.[12] Although the aforementioned chemical synthesis method can be used for large-scale preparation of MoS_2 nanosheets, the synthetic conditions are rigid in which inert gas is usually required, and the ligands coated on MoS_2 nanosheets are difficult to remove and thus seriously detrimental to the electron transport, largely restricting their applications in catalysis and electronics.

2.6. Sorting and Separation Strategies

The solution-processed MoS_2 nanosheet is easily sorted and separated, which is one of the distinct features compared to those prepared by mechanical and CVD methods. Generally, the prepared MoS_2 nanosheets in solution exhibit broad lateral size distribution and various thicknesses. As known, the physical and electronic properties of MoS_2 nanosheets greatly depend on their size and thickness. Therefore, preparation of MoS_2 nanosheets with uniform size and thickness is extremely important for practical applications. Until now, strategies for sorting MoS_2 nanosheets have been developed, mainly including the sedimentation-based separation and density-gradient ultracentrifugation.

Sedimentation-based separation is one of the most commonly used methods for separation of 2D nanomaterials, which has been used for sorting MoS_2 flakes with various size and thickness.[11a,14a,b] It relies on the different sedimentation rate of flakes in response to a centrifugal force. Typically, large flakes with relatively heavy weight can be easily precipitated under centrifugation, while small ones with light weight prefer to stay in the top of dispersion. The process of sedimentation-based separation is described as follows: A MoS_2 suspension is filled in a centrifuge tube, which is then used for centrifugation. In analogy with previous sorting experiments for graphene,[14a,b] the large-size MoS_2 flakes with heavy weight could precipitate much faster than the exfoliated single-layer MoS_2 nanosheets. Consequently, once the centrifugation is complete, the different sized MoS_2 is separated, that is, the largest MoS_2 flakes with heaviest weight are located at the bottom of the centrifuge tube, while the exfoliated nanosheets stay near the top. Therefore, this method is quite efficient to remove the non-exfoliated and large-size MoS_2 flakes. Importantly, this separation process greatly depends on the property of the dispersion solvent. For instance, MoS_2 nanosheets in NMP have averagely larger size compared to those in water/surfactant dispersions because of their different viscosities. The viscosity of NMP (1.7 MPa s) is higher than that of water (ca. 1 MPa s) at room temperature. Large flakes dispersed in high-viscosity medium have large frictional force which reduces their sedimentation coefficient, making them difficult to precipitate.[39] To date, this method is the most common strategy for the separation of MoS_2 nanosheets.

Density-gradient ultracentrifugation is another method used for separation of mixtures with different buoyant densities.[40] Typically, samples and liquids are mixed in a centrifuge tube to form a spatially varying density profile. Upon high-speed centrifugation, the samples are separated into different regions with different individual densities. Importantly, the density-gradient ultracentrifugation can be performed in both aqueous and organic solvents and does not require a stationary phase. However, this method is rarely used for sorting MoS_2 nanosheets because of the high intrinsic buoyant density of MoS_2. Hersam et al. solved this problem by using an amphiphilic block copolymer (Pluronic F68) dispersant as the surfactant (Figure 2).[40b] This copolymer is composed of a central hydrophobic unit flanked by hydrophilic chains, which greatly reduce the overall buoyant density in aqueous solution. In their work, MoS_2 was first exfoliated and dispersed in the aqueous solution of copolymer. After

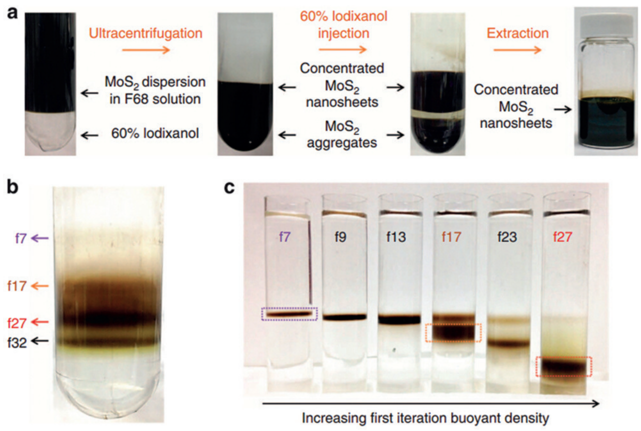

Figure 2. a) Photographs of the concentration steps for MoS_2 nanosheets. b) Photograph of MoS_2 bands in an ultracentrifuge tube after the first iteration of density-gradient ultracentrifugation. c) Photograph of the ultracentrifuge tubes after the second iteration of density-gradient ultracentrifugation. Reproduced with permission from Ref. [40b]. Copyright 2014, Nature Publishing Group.

 © 2016 Wiley-VCH Verlag GmbH & Co. KGaA, Weinheim

centrifugation of the dispersion, iodixanol solution containing F68 was injected to the sediment to separate and fractionate the concentrated MoS_2 nanosheets (Figure 2a). Subsequently, the fractionated F68–MoS_2 solution was ultra-centrifuged two times, allowing the formation of well-defined MoS_2 bands at their corresponding isopycnic points (Figure 2b,c). The thickness-sorted MoS_2 is highly crystalline with low defects. Interestingly, the thickness sorting of MoS_2 nanosheets from the most buoyant single-layer nanosheets shows the emerging photoluminescence.

3. MoS_2 Nanosheet-Based Hybrids

As one of the most studied TMD nanomaterials, MoS_2 nanosheets have been used as building blocks or supports for the preparation of composites with other materials, such as organic and bio-materials,[5d,6e,41] noble metals,[7a,c,42] metal oxides,[43] metal chalcogenides,[44] graphene,[45] and other carbon nanomaterials.[46] Moreover, the synergetic effect arising from two or multiple components can trigger some enhanced properties or improved performances.

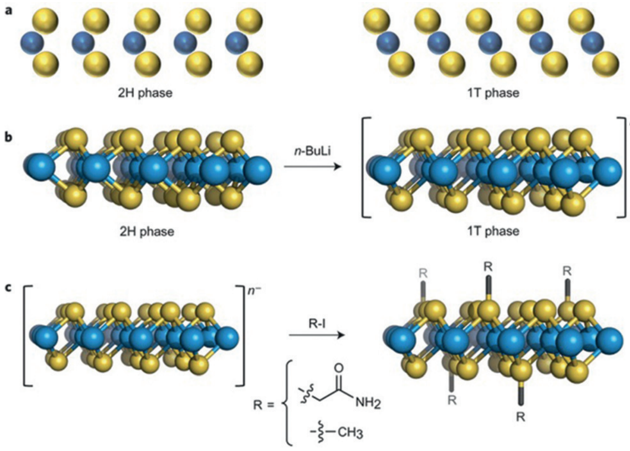

Figure 3. a) Schematic illustration of side view of 2H and 1T phases of MoS_2. b) The 2H phase of MoS_2 is converted into the 1T phase via lithiation using butyllithium (BuLi). The 1T phase is negatively charged. n^- indicates the excess charges carried by the exfoliated 1T-phase nanosheets. c) The nanosheets are functionalized using 2-iodoacetamide or iodomethane (R–I) solution. Reproduced with permission from Ref. [41a]. Copyright 2015, Nature Publishing Group.

3.1. Hybrids of MoS_2 Nanosheets and Organic/Bio-Materials

The absence of dangling bonds on MoS_2 basal plane makes it difficult to modify MoS_2 nanosheets with functional groups. Therefore, great efforts have been devoted to conjugate organic ligands on the surface of MoS_2 nanosheets.[41a,b,d] For example, Dravid and co-workers proposed a facile ligand conjugation method to functionalize MoS_2 nanosheets with thiol ligands.[41b] This functionalization was achieved by conjugation of thiols at the sulfur vacancy sites and edge defects. Three functional groups, including -OH, -COOH, and NMe_3^+, were conjugated on the surface of chemically exfoliated MoS_2 nanosheets through the connection of thiol chain, which have suitable ligand affinities with the defects of MoS_2 nanosheets. Importantly, the surface potential and functionality of the hybrids can be readily controlled to form versatile MoS_2-based composites. In another example, McDonald and co-workers conjugated $M(OAc)_2$ (M = Ni, Cu, Zn; OAc = acetate) on MoS_2 nanosheets through covalent functionalization using surface modification techniques.[41d] Typically, the 2-propanol (IPA)-assisted liquid exfoliated 2H-MoS_2 nanosheets were allowed to react with carboxylate salts in IPA solution. The coordination interaction between the surface S atoms of MoS_2 and the metal center of $M(OAc)_2$ induces the functionalization and formation of hybrids. Moreover, Chhowalla and co-workers demonstrated that 1T-MoS_2 nanosheets can be selectively modified through conjunction of iodoacetamide compounds (Figure 3).[41a] Specifically, MoS_2 nanosheets with 65% 1T phase were prepared via the lithiation intercalation method using *n*-butyllithium as the intercalator (Figure 3b). After reaction with ten-fold excess 2-iodoacetamide in water for 5 days, the functional groups were directly attached on the electron-rich 1T metallic MoS_2 nanosheets, forming covalently functionalized composites (Figure 3c). This functionalization was realized by the efficient electron transfer between electron-rich 1T MoS_2 nanosheets and organohalide reactant, which resulted in the organohalide being covalently grafted onto MoS_2 nanosheets, instead of the conventional physical adsorption on defect sites of MoS_2. Amazingly, after the functionalization process, the properties of 1T phase were dramatically changed from metallic to semiconducting, leading to a strong and tunable photoluminescence. Using a similar procedure, that is, lithium intercalation, chemical exfoliation and subsequent quenching of the negative charges of MoS_2 by strong electrophiles, Claudia and co-workers functionalized organic groups onto chemically exfoliated MoS_2 nanosheets via covalent C–S bonding.[47] The degree of functionalization is 10–20 atom%, which can be tuned by the intercalation conditions.

Besides the surface functionalization through ligand conjunction process, MoS_2 nanosheets with large surface areas can be a good template to hybridize with organic materials.[5d,22,48] As a typical example, our group reported that single-layer MoS_2 nanosheet can be used as a template for directing the assembly of organic aggregation-induced emission (AIE) molecules (4,6-di(9H-carbazol-9-yl)-*N*,*N*-diphenyl-1,3,5-triazin-2-amine (DDTA)).[48] With the assistance of MoS_2 nanosheets, the AIE molecules could be assembled into organic nanosheets with size of about 0.2–2 μm and thickness of about 9–20 nm. Interestingly, the fluorescence intensity of AIE molecules was greatly enhanced instead of quenched by MoS_2 nanosheets.

In addition to organic materials, MoS_2 nanosheets have also been hybridized with polymers through physical adsorption and/or van der Waals force interaction. For example, our group demonstrated the preparation of PVP-coated MoS_2 nanocomposite, that is, MoS_2-PVP, by direct sonication of MoS_2 bulk crystal in PVP ethanolic solution.[5d] The average thickness and lateral size of MoS_2-PVP composite is about

 © 2016 Wiley-VCH Verlag GmbH & Co. KGaA, Weinheim

3 nm and a few hundreds of nanometers, respectively. Significantly, because there are hydrophobic methylene groups and hydrophilic amide groups on PVP, the MoS_2-PVP composite can be dispersed in various solvents, such as water, ethanol, chloroform, THF, and acetone. Besides the surface-coating ability, polymers have also been used to engineer the morphology and architectures of MoS_2-based composites. Very recently, our group reported the formation of chiral MoS_2-polymer nanofibers based on the self-assembly of MoS_2 nanosheets in highly stirred polymeric P123 solution (Figure 4a–c).[41e] The MoS_2-P123 composite showed a left-handed chiral structure with a length of about 10–50 μm and diameter of around 10–50 nm. Moreover, the chiral nanofibers could be further reassembled into nanorings with diameter of approximately 400–600 nm. As another way to prepare MoS_2-polymer composites, MoS_2 nanosheets have been used as templates to adsorb organic monomers, and then direct the growth of polymers. For example, the Tang group prepared the polypyrrole (PPy)-MoS_2 nanocomposite by polymerization of pyrrole monomers in the presence of exfoliated MoS_2 nanosheets.[41i] The strong coordination interaction between pyrrole monomers and MoS_2 nanosheets contributes to the homogeneous polymerization process, enabling the formation of PPy ultrathin films on MoS_2 surface.

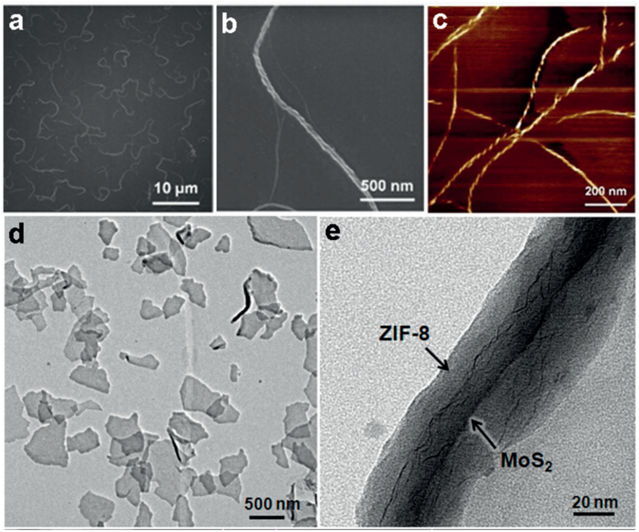

Figure 4. a),b) SEM images and c) AFM phase image of chiral MoS_2 nanofibers. Reproduced with permission from Ref. [41e]. Copyright 2015, American Chemical Society. d) TEM image of MoS_2@ZIF-8 hybrid structures. e) TEM image of a MoS_2@ZIF-8 structure, showing the curled MoS_2 nanosheets (core) and the ZIF-8 coating (shell). Reproduced with permission from Ref. [50a]. Copyright 2014, American Chemical Society.

Moreover, bio-molecules and bio-materials have also been hybridized with MoS_2 nanosheets.[6e,41f,h] As a typical example, our group demonstrated that the single-layer MoS_2 nanosheet was a good template to absorb DNA molecules via van der Waals interaction between nucleobases of DNA and the basal plane of MoS_2.[6e] Similarly, Chu and co-workers prepared DNA–MoS_2 hybrid nanomaterials via a short-time reaction of specific aptamer probes and MoS_2 nanosheets.[41h] The aptamers can be easily absorbed on the MoS_2 surface through van der Waals interactions. The resulting hybrid nanosheets exhibit thickness of about 1.6 nm. Furthermore, Zhao and co-workers demonstrated the preparation of chitosan (CS)-functionalized MoS_2 (MoS_2-CS) nanosheets via a modified oleum-treated liquid-phase exfoliation method in the presence of chitosan.[41f] The thickness of MoS_2-CS nanosheets increased to about 4–6 nm compared to the pristine single-layer MoS_2 nanosheets, and the lateral size of MoS_2-CS hybrids is around 80 nm. Importantly, the MoS_2-CS nanosheets can be dispersed in water and other physiological buffers with high stability and biocompatibility, showing great potential in biomedicine.

3.2. Hybrids of MoS_2 Nanosheets and Metal–Organic Frameworks (MOFs)

MOFs are compounds in which metal ions are linked by coordinating organic species.[49] Among MOFs, ZIF-8 is particularly attractive for hybridization with MoS_2 nanosheets owing to its chemical and thermal stability.[50] Recently, our group demonstrated that ZIF-8 can be grown and coated on MoS_2 nanosheets to form 2D MoS_2@ZIF-8 core–shell hybrid structure (Figure 4d,e).[50a] The MoS_2 nanosheets act as templates to direct the growth and coating of ZIF-8 on MoS_2. The thickness of ZIF-8 layer in the hybrid core–shell structure is about 80 nm, and it can be tuned by the concentration of precursors and the reaction time. Additionally, this general method is also feasible for coating ZIF-8 on other 2D materials such as graphene oxide (GO) and reduced graphene oxide (rGO) nanosheets, and their hybrids with metal nanoparticles (NPs) (i.e., Pt-GO, Pt-rGO, and Pt-MoS_2 hybrids). Similarly, Golberg and co-workers also reported the preparation of ZIF-8 wrapped MoS_2, which was then used as template to prepare MoS_2@microporous carbon composites for supercapacitors.[50b] In addition, another kind of MOF structure, that is, UiO-66, has been reported to hybridize with MoS_2 and CdS for photocatalytic H_2 production.[51]

3.3. Hybrids of MoS_2 Nanosheets and Metals or Metal Oxides

The solution-processed MoS_2 nanosheets are suitable support for noble-metal nanocrystals. Up to now, several types of noble-metal nanostructures, including Pt,[7a,42a] Pd,[7a,42a] Ag[7a,42a,b] and Au,[7c,42a,c–f] have been grown on MoS_2 nanosheets. As a typical example, for the first time, our group developed a solution-based method for the epitaxial growth of noble metals, including Pd, Pt, and Ag, on single-layer MoS_2 nanosheets.[7a] After reduction of K_2PdCl_4 with ascorbic acid in the presence of PVP and MoS_2 nanosheets, Pd NPs with the size of around 5 nm were perfectly grown on the surface of MoS_2 nanosheets epitaxially (Figure 5a,b). Similarly, Pt NPs with the size of 1–3 nm were epitaxially grown on MoS_2 nanosheets via the photochemical reduction of K_2PtCl_4 in the presence of sodium citrate

 © 2016 Wiley-VCH Verlag GmbH & Co. KGaA, Weinheim

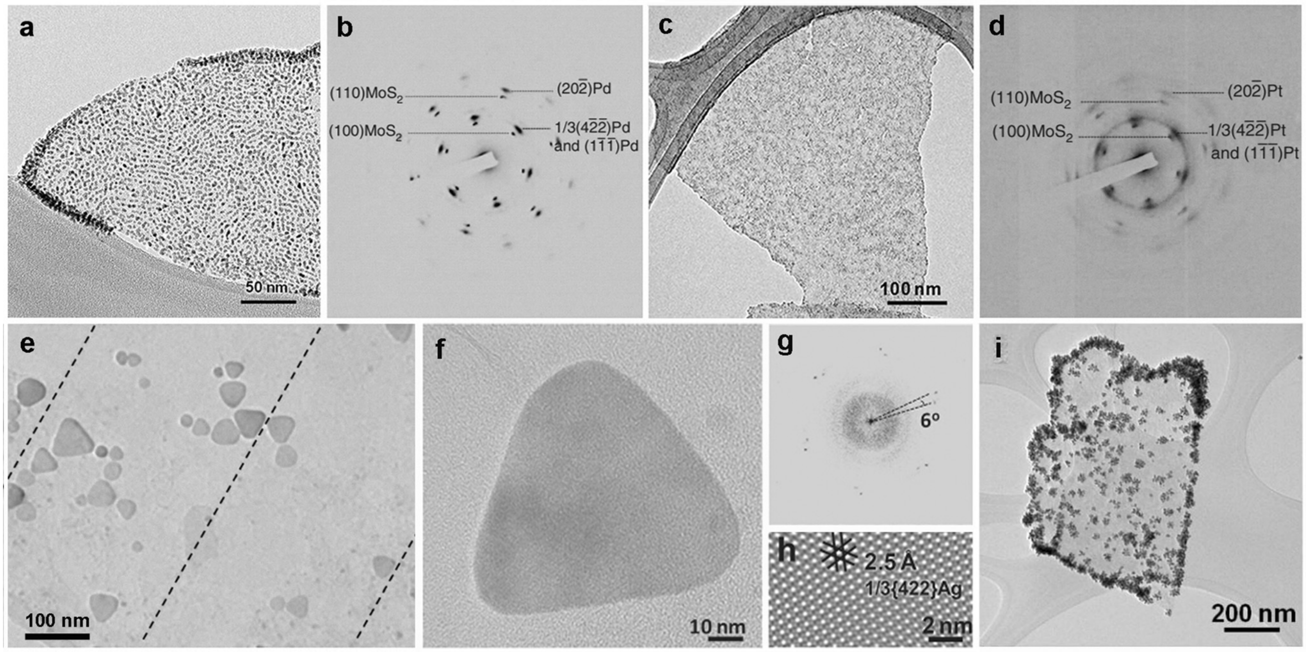

Figure 5. a) TEM image of Pd NPs synthesized on a MoS_2 nanosheet. b) SAED pattern of a Pd–MoS_2 hybrid nanosheet with the electron beam perpendicular to the basal plane of the MoS_2 nanosheet. c) TEM image of Pt NPs synthesized on a MoS_2 nanosheet. d) SAED pattern of a Pt–MoS_2 hybrid nanosheet with the electron beam perpendicular to the basal plane of the MoS_2 nanosheet. e) TEM image of Ag nanoplates synthesized on a MoS_2 nanosheet. f) TEM image of a typical Ag nanoplate on a MoS_2 nanosheet. g) Fast Fourier transform generated SAED pattern of (f). (h) Filtered HR-TEM image of the Ag nanoplate in (f). i) TEM image of Au NPs synthesized on a MoS_2 nanosheet. Reproduced with permission from Ref. [7a]. Copyright 2013, Nature Publishing Group.

(Figure 5 c,d). Silver triangular nanoplates were epitaxially grown on MoS_2 nanosheets in the presence of CTAB or PVP (Figure 5 e–h). Note this was the first example of the solution-based epitaxial growth of noble metals on single-layer MoS_2. Moreover, it was found that Au NPs grew randomly on MoS_2 nanosheets (Figure 5 i), because the reduction of Au^{3+} was finished within several seconds in the MoS_2 dispersion.[7a,42e,f] The spontaneous reduction of Au NPs on MoS_2 nanosheets was also reported by the Yang group[42f] and Huang group.[42e] It was suggested that the Fermi level of MoS_2 is situated above the reduction potential of $AuCl_4^-$ (+1.002 V versus the standard hydrogen electrode (SHE)), leading to the spontaneous electron transfer from MoS_2 to $AuCl_4^-$, which gives rise to the formation of Au NPs on MoS_2 surface.[42e]

Besides noble metals, metal oxide nanomaterials, such as MoO_3,[43a,b,h,i,52] TiO_2,[43c,d] Fe_3O_4,[43e] and SnO_2,[43f,g] have also been hybridized with MoS_2 nanosheets. It is noteworthy that MoS_2 nanosheets, especially those with single-layer atomic thickness, are not stable in air, and can be easily oxidized to MoS_2-MoO_x composites. For example, Xie and co-workers reported the synthesis of oxygen-incorporated ultrathin MoS_2 nanosheets by the simple hydrothermal treatment of $(NH_4)_6Mo_7O_2{\cdot}4H_2O$ and thiourea.[7e] The ultrathin composites showed lateral size of 100–200 nm and thickness of 5–10 nm. Importantly, the oxygen incorporation greatly enhances the intrinsic conductivity of nanosheets by reducing the band gap of MoS_2 from 1.75 eV to 1.30 eV. As another typical example, our group developed a facile two-step method for fabrication of MoO_3-MoS_2 hybrid materials by using the heat treatment of electrochemically exfoliated MoS_2 nanosheets.[43h] The MoS_2 nanosheets were partially oxidized in situ by a heat-assisted spray-coating process in air during the film preparation, and the subsequent thermal-annealing-driven crystallization induced the formation of the MoO_3-MoS_2 composite. The hybrid nanomaterial was composed of (100)-dominated MoS_2 and (021)-α-dominated MoO_3. This facile method without any complicated processes or additional reagents could be extended to prepare other types of MS_2/MO_x composites. In a similar fashion, Bessonov and co-workers recently demonstrated the preparation of MoO_x/MoS_2 heterostructures.[43a] Briefly, the MoS_2 films were first collected from the mixed solvents of ethanol and hexane by using a modified Langmuir–Blodgett method. After drying in a vacuum oven, the MoS_2 films were then heated in air on a hot plate at 150–200 °C for 3–10 h. Because the oxygen diffusion is limited, the annealing process gave rise to a MoO_x layer approximately 3 nm thick on the MoS_2 film surface, thus forming the MoO_x/MoS_2 heterostructures. Recently, Kim and co-workers demonstrated another one-step oxidation/exfoliation method to directly prepare bi- or tri-layer MoO_3/MoS_2 composites.[43b] H_2O_2 was first used to penetrate MoS_2 interlayers and oxidize bulk MoS_2 to form the expanded MoS_2 with MoO_3 NPs, which was then sonicated in aqueous solution to obtain the MoO_3/MoS_2 composites.

Besides the aforementioned methods, other methods have also been developed for the hybridization of metal oxides with MoS_2 nanosheets. For instance, our group developed a facile method for fabrication of 3D hierarchical MoS_2-

 © 2016 Wiley-VCH Verlag GmbH & Co. KGaA, Weinheim

coated TiO_2 nanobelts via a simple hydrothermal reaction.[43c] Specifically, the mixture of sodium molybdate ($Na_2MoO_4{\cdot}2H_2O$) and thioacetamide (C_2H_5NS) was hydrothermally treated at 200 °C for 24 h with pre-synthesized TiO_2 nanobelts as the template. Note that the TiO_2 nanobelts can effectively inhibit the growth of MoS_2 along the *c*-axis, leading to the formation of TiO_2@MoS_2 heterostructures. Most of the MoS_2 nanosheets grown on TiO_2 nanobelts had the thickness of about 5 nm, that is, less than 7 layers. As another example, Xue and co-workers reported the fabrication of ultra-small Fe_3O_4 NPs decorated MoS_2 nanosheets, that is, Fe_3O_4/MoS_2 composites, via a two-step hydrothermal method.[43e] In the first step, the MoS_2 nanosheets were prepared by a hydrothermal method using Na_2MoO_4 and C_2H_5NS as precursors. The obtained MoS_2 nanosheets were subsequently used as templates to grow Fe_3O_4 NPs via the hydrothermal treatment of iron chloride hexahydrate ($FeCl_3{\cdot}6H_2O$), sodium bicarbonate ($NaHCO_3$), and L-ascorbic acid, forming the Fe_3O_4/MoS_2 composites. It was found that ultra-small Fe_3O_4 NPs with average size of about 3.5 nm were uniformly deposited on few-layer MoS_2 nanosheets. Similarly, an SnO_2/MoS_2 composite was also prepared via a two-step hydrothermal method.[43f] The SnO_2 NPs were grown on the MoS_2 nanosheets, and acted as spacers to prevent the restacking of the MoS_2 nanosheets.

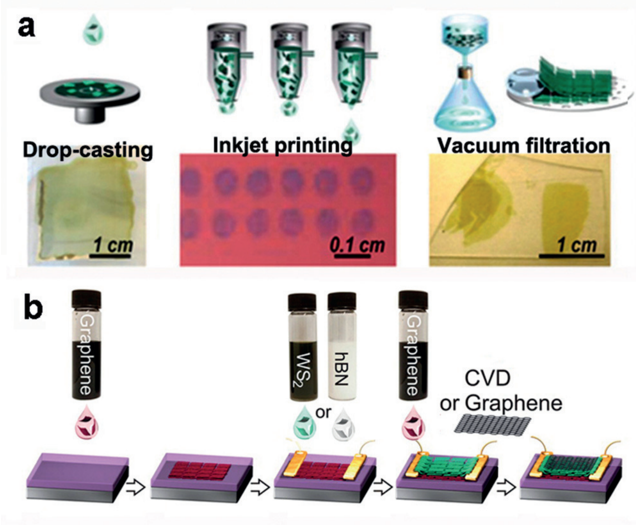

Figure 6. a) Schematic illustration of deposition methods for liquid-phase exfoliated 2D atomic crystals and the optical micrographs of deposited films: drop-casting on glass, inkjet printing on Si/SiO_2 (300 nm), vacuum filtration, and fishing on glass. b) Schematic illustration of a general fabrication process for heterostructure devices by using 2D-crystal inks. Reproduced with permission from Ref. [44d]. Copyright 2014, American Chemical Society.

3.4. Hybrids of MoS_2 Nanosheets and Metal Chalcogenides

The large variety of TMD nanosheets offers a rich platform for the construction of versatile heterostructures which can combine the merits of the individual materials. Typically, the liquid-phase process offers advantages for the layer-by-layer hybridization of nanosheets. For example, Rajamathi and co-workers demonstrated the hybridization of MoS_2 and WS_2 nanosheets by a layer-by-layer restacking method.[44c] During a typical process, ammoniated MS_2 (M = Mo, W) were prepared by reaction of Li_xMS_2 with a saturated solution of ammonium chloride (NH_4Cl), followed by a subsequent sonication-assisted exfoliation process. After evaporation of the solvent from the colloidal dispersion consisting of ammoniated MoS_2 and WS_2 nanosheets, the MoS_2/WS_2 composite was formed. However, the composition of the hybrids was difficult to control because the nanosheets were just randomly stacked together. The hybrids degraded slowly within several days, which severely limited their applications. Recently, Casiraghi and co-workers carried out three different methods, that is, drop-casting, inkjet printing, and vacuum filtration, for the fabrication of 2D heterostructures via the layer-by-layer technique using liquid inks (Figure 6).[44d] The three methods have been proved to be effective for the deposition of flat, dense, and pinhole-free films in liquid phase. Moreover, the composition and functionality of resultant 2D hybrid materials can be fine-tuned by changing the properties of the ink and solvents. In comparison, each method shows specific characteristics and advantages. The drop-casting method is able to produce large area films and the pinholes can be minimized by using high concentration dispersions. The inkjet printing method can effectively control the shape of the films and reduce the pinholes by repeating printing process. Compared to the drop-casting method, the vacuum filtration process can well control the pinhole density by repeating the transfer several times on the same area.

Besides 2D TMD nanosheets, other kinds of metal chalcogenides, such as CdS[44b] and PbSe,[44a] have also been hybridized with MoS_2 nanosheets. Very recently, we reported the synthesis of MS_2-CdS nanohybrids (M = Mo or W) through a one-pot wet chemical method.[44b] The particle size of WS_2-CdS and MoS_2-CdS nanohybrids is 4–10 nm and 6–11 nm, respectively. Interestingly, single-layer MoS_2 nanosheets with the thickness of 0.4 nm and lateral size less than 10 nm were found to selectively grow on the Cd-rich (0001) surface of Wurtzite CdS nanocrystals. This unique structure exposed a large number of active edges of single-layer MoS_2 and thus exhibiting excellent photocatalytic activity. As another example, Zaumseil and co-workers developed a facile hot-injection method for growth of MoS_2-PbSe hybrids, in which the PbSe QDs with average size of 5.7 nm were in situ epitaxially grown on the exfoliated MoS_2 nanosheets.[44a] Because of the protection by the surface oleic acid ligands, the hybrid materials are stable in ambient conditions.

3.5. Hybrids of MoS_2 Nanosheets and Carbon Materials

Because of the good chemical stability and excellent flexibility, carbon materials, including graphene and its derivatives,[45a,l,m,q,53] carbon nanotubes (CNTs)[46c–e,54] and carbon fibers,[46f,g,55] have been widely used for hybridization with MoS_2 nanosheets. Specifically, chemically treated carbon materials, such as GO and rGO, usually have abundant

 © 2016 Wiley-VCH Verlag GmbH & Co. KGaA, Weinheim

oxygen-containing groups that can easily react/assemble with other components to form hybrid materials.[56] The assembly of MoS_2 nanosheets with graphene or its derivatives has been reported by several groups.[45a,l,m,q,53] For example, Chen and co-workers reported the synthesis of layered MoS_2/graphene 3D hybrid nanostructures by hydrothermal treatment of $Na_2MoO_4{\cdot}2\,H_2O$ and GO, with the assistance of L-cysteine.[45a] Particularly, after post-annealing treatment in H_2/N_2 atmosphere at 800 °C for 2 h, the MoS_2/graphene composite delivered a 3D sphere-like architecture consisting of curved nanosheets. Interestingly, the intensity of all the X-ray diffraction (XRD) peaks of MoS_2, especially the (002) plane, decreased with increasing graphene content, indicating that the addition of graphene inhibited the growth of layered MoS_2 in the composites, especially in the (002) plane. In addition, Wu and co-workers demonstrated that the p-type MoS_2/n-type nitrogen-doped rGO (NRGO) heterostructures can be prepared by the reaction of rGO and $(NH_4)_2MoS_4$, followed by a post-heating in NH_3 flow.[57] p-Type MoS_2 nanoplates with size of 5–20 nm were deposited on the surface of NRGO, forming lots of nanoscale p–n junctions. Importantly, the design strategy can be extended beyond MoS_2 and rGO to form versatile heterostructures. Different from the aforementioned hydrothermal method, two promising approaches, that is, layer-by-layer assembly and spinning process, have also been developed for preparation of the hybrids based on MoS_2 nanosheets. Typically, the hybrid nanostructure prepared by layer-by-layer approach usually demonstrates a thin-film or sheet-like structure, while spinning process gives rise to a fiber-like structure. For example, Casiraghi and co-workers reported the preparation of MoS_2/GO or rGO hybrid films using three different methods, that is, drop-casting, inkjet printing, and vacuum filtration, which share the same procedure to prepare MoS_2-metal chalcogenide hybrids and have been mentioned before (Figure 6 b).[44d] In addition, our group developed a spinning process for the synthesis of ultra-long microfiber from the mixture of rGO and TMD nanosheets.[45n] Briefly, the aqueous dispersion of TMD nanosheets was mixed with GO with a vortex mixer, followed by a spinning process to form the hybrid fibers. After reducing GO to rGO by using hydroiodic acid, the TMD-rGO hybrid fibers were obtained. This method does not involve any special reagents and complex process, which shows great potential in the fabrication of fiber-based composites. Moreover, the MoS_2/graphene composites have also been used as templates for formation of ternary hybrid materials.[44d,58] Recently, Jaroniec and co-workers reported a two-step hydrothermal approach to grow TiO_2 on MoS_2/graphene hybrid nanosheets, forming a ternary TiO_2/MoS_2/graphene composite.[58b] The layered MoS_2/graphene hybrid was first synthesized by hydrothermally treating Na_2MoO_4 and H_2CSNH_2 in a GO solution. After that, the as-formed MoS_2/graphene reacted with $Ti(OC_4H_9)_4$ through a second hydrothermal reaction, giving rise to the TiO_2/MoS_2/graphene composite, in which TiO_2 nanocrystals with average size of 7–10 nm were deposited on the MoS_2/graphene hybrid. Similarly, another 2D porous ternary MoS_2-based composite consisting of graphitic C_3N_4 nanosheets, nitrogen-doped graphene, and layered MoS_2, referred to as CNNS/NRGO/MoS_2, was prepared by Chen and co-workers recently.[58a]

Besides graphene, the CNTs,[46c–e,54] carbon fibers[46f,g,55] and other forms of carbon materials[46g] have also been hybridized with MoS_2 nanosheets. For instance, Lou and co-workers demonstrated a facile glucose-assisted hydrothermal method for direct growth of ultrathin MoS_2 nanosheets on acid-treated CNTs.[46d] MoS_2 nanosheets with thickness of 5–10 nm were grown on the CNT backbone. Impressively, the glucose not only assisted the formation of MoS_2 nanosheets, but also acted as binder to boost the growth of MoS_2 nanosheets on CNTs with uniform coverage along the longitudinal axis. As another example, the nanocomposite consisting of MoS_2 and multi-walled carbon nanotubes (MWCNT@MoS_2) was synthesized by annealing a mixture of MWCNTs and MoS_2 in a H_2 atmosphere.[46c] Moreover, Yu and co-workers reported the preparation of carbon nanofibers decorated with MoS_2 nanosheets (CNF@MoS_2) through a facile hydrothermal method by using low-cost biomass-derived carbonaceous nanofibers as the support.[46f] The CNF@MoS_2 has a cable-like structure with diameter of 100 to 140 nm. Recently, our group fabricated ternary hybrid fibers consisting of MoS_2, rGO, and MWCNTs by incorporation of MoS_2 and rGO nanosheets into the well-aligned MWCNT sheet followed by twisting.[59] The continuous MWCNT sheet was first pulled out from the vertically aligned MWCNT array. After drop-casting MoS_2 and GO nanosheets onto the MWCNT sheet, the resulting hybrid was dried and twisted by using an electric motor to give the MoS_2/GO/MWCNT fiber. Finally, the hybrid fiber was reduced by hydroiodic acid to obtain the ternary MoS_2/rGO/MWCNT fiber. This method is very simple and reproducible, which can also be used for fabrication of fiber-like CNT/MoS_2-based composites.

4. Applications

4.1. Electrocatalysis

Electrocatalysis is one of the most promising applications for solution-processed MoS_2 nanosheets, especially for the electron-driven hydrogen-evolution reaction (HER). Compared with the traditional noble-metal catalysts (e.g. Pt NPs), the MoS_2 nanosheet is a promising non-precious candidate because of its low cost, high chemical stability, and good catalytic performance toward HER.[7f,60] However, owing to the limited active sites, inefficient electrical contact with catalysts, and intrinsic poor electrical transport property, the catalytic performance of pure MoS_2 is not as good as expected. Therefore, different strategies have been developed to improve the catalytic performance of MoS_2 nanosheets.

1) Engineering the effective active sites of MoS_2 nanosheets. The active site is one of the key parameters to determine the performance of a catalyst. Therefore, engineering the MoS_2 structure at the atomic scale or tailoring MoS_2 nanosheets into smaller segments should be considered. For example, mesoporous MoS_2 with a double-gyroid morphology has been designed to expose more edge atoms as the active

© 2016 Wiley-VCH Verlag GmbH & Co. KGaA, Weinheim

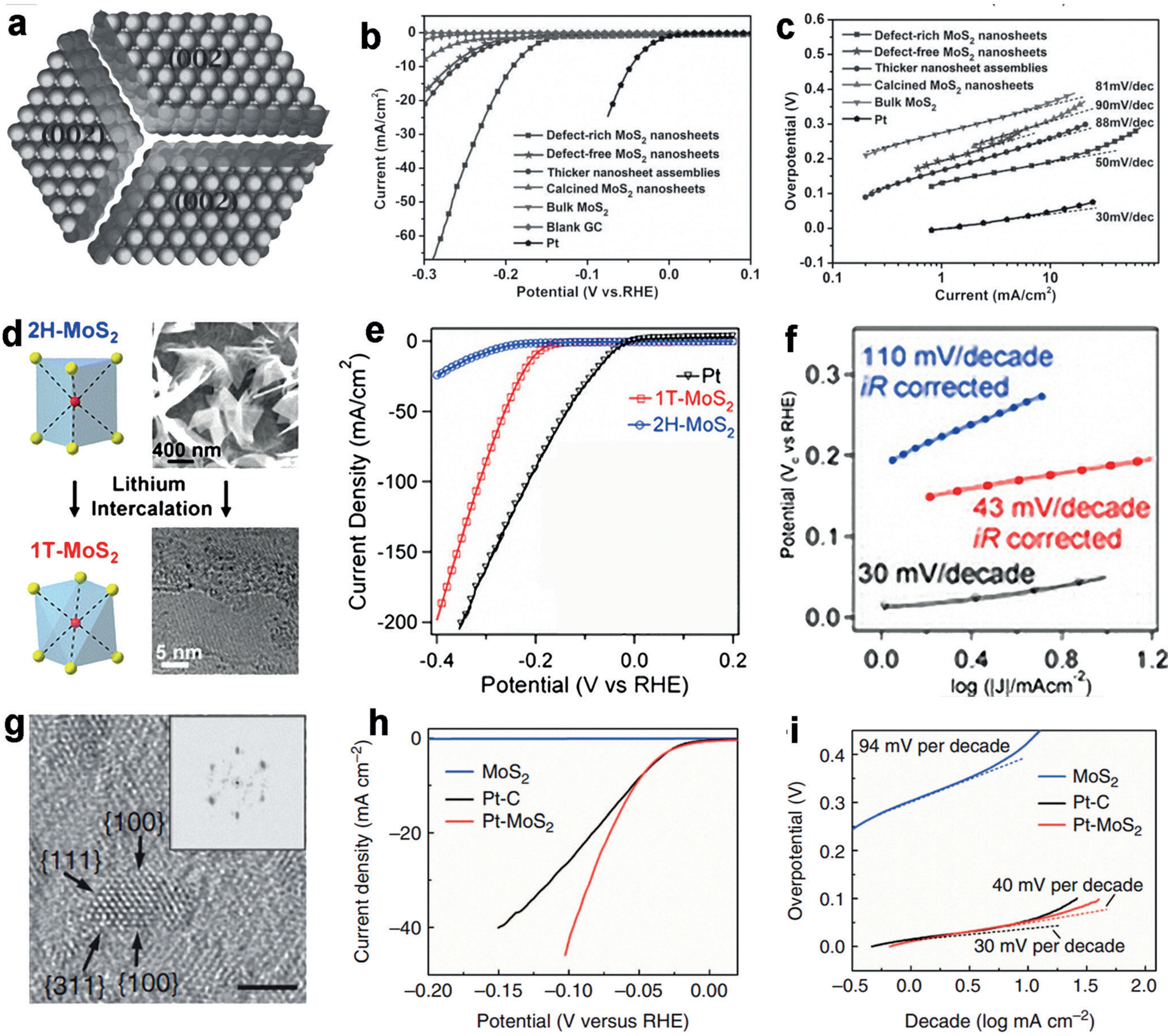

Figure 7. a) Atomic reconstruction of defect-rich MoS_2 ultrathin nanosheets. b) Polarization curves of various samples and c) the corresponding Tafel plots. Reproduced with permission from Ref. [37]. Copyright 2013, John Wiley & Sons, Inc. d) 2H and 1T models of MoS_2, and the corresponding top-down SEM image of as-grown 2H-MoS_2 and HR-TEM image of chemically exfoliated 1T-MoS_2 nanosheets. e) Polarization curves of 1T-MoS_2, 2H MoS_2, and Pt, and f) the corresponding Tafel plots. Reproduced with permission from Ref. [65b]. Copyright 2013, American Chemical Society. g) HR-TEM images of (101)-oriented Pt NPs on MoS_2 (scale bar, 2 nm). h) Polarization curves of Pt/MoS_2, Pt/C and MoS_2, and i) the corresponding Tafel plots. Reproduced with permission from Ref. [7a]. Copyright 2013, Nature Publishing Group.

sites.[61] Similarly, the small-sized MoS_2 nanodots and other architectures[62] have been synthesized with increased fraction of edge sites, which gives enhanced electrocatalytic activity. As a typical example, Xie and co-workers prepared defect-rich MoS_2 nanosheets and highlighted the importance of active edges for HER (Figure 7a–c).[37] Interestingly, the existence of defects in MoS_2 nanosheets results in partial cracking of the basal planes, and thus leads to exposure of additional active edge sites. Compared to the defect-free MoS_2 nanosheets, the defect-rich MoS_2 ultrathin nanosheets exhibited much improved HER performance, that is, small onset over-potential of 120 mV (Figure 7b), large cathodic current density, small Tafel slope of 50 mV decade^{-1} (Figure 7c), and superior electrochemical cycling stability. As another example, Sun and co-workers reported the synthesis of edge-terminated MoS_2 nanosheets with expanded interlayer spacing through a microwave heating strategy.[63] The obtained MoS_2 exhibited excellent kinetic metrics with the onset potential of −103 mV, Tafel slope of 49 mV decade^{-1} and exchange current density of 9.62×10^{-3} mA cm^{-2}.

2) Engineering the intrinsic electrical conductivity of MoS_2 nanosheets. The low conductivity of MoS_2 mainly arises from its inherent structure in which there is van der Waals interaction between two adjacent S-Mo-S sheets. The electrical resistivity across different layers has been measured to be 2200 times greater than that within the layer.[64] This suggests that the single-layer MoS_2 is an optimal structure because the electron transmission is most efficient. Recently,

 © 2016 Wiley-VCH Verlag GmbH & Co. KGaA, Weinheim

Cao and co-workers demonstrated the layer-dependent electrocatalysis of MoS_2 for HER by using CVD-grown MoS_2, and concluded that the layer dependence is rooted in the interlayer hopping of electrons.[7d] Moreover, experiment results suggested that not only the edge sites, but also the basal plane atoms are active sites. Alternatively, increasing the ratio of metallic MoS_2 is another feasible and promising way to enhance the electrical conductivity. As known, the Li-intercalation of MoS_2 (Li_xMoS_2) will induce the structure transformation of MoS_2 from the 2H phase to the 1T phase, along with a change from being semiconducting to metallic. Jing and co-workers demonstrated that metallic 1T-MoS_2 could greatly improve the HER catalytic performance.[65] Briefly, the 1T-MoS_2 nanosheets were prepared by lithium intercalation of the semiconducting 2H-MoS_2 grown on graphite substrates (Figure 7 d).[65b] Experimental results confirmed that this catalyst exhibited facile electrode kinetics and low-loss electrical transport with a Tafel slope of 43 mV decade^{-1} (Figure 7 e,f). Importantly, the catalytic performance of 1T-MoS_2 nanosheets is stable and there is a less than 15 % decay of the electrocatalytic current density after 1000 cycles. Recently, Chhowalla and co-workers also demonstrated that metallic MoS_2 nanosheets exhibited superior catalytic activity toward the hydrogen evolution with a notably low Tafel slope of 40 mV decade^{-1}.[66] Different from the conventional *n*-butyllithium intercalators, lithium borohydride ($LiBH_4$) was used as the lithium source and the ratio of 1T-MoS_2 was achieved as high as 80 %. Interestingly, by partially oxidizing the exfoliated MoS_2 nanosheets, it was found that the catalytic activity of 2H-MoS_2 was significantly reduced, while 1T-MoS_2 was completely unaffected. Normally, the oxidation process initiates at the edges of MoS_2 nanosheets which are the catalytic active sites for HER. The unaffected HER performance of 1T-MoS_2 suggested that the edges of metallic MoS_2 nanosheets are not the main active sites, while their basal plane is catalytically active. Differently, Xie and co-workers demonstrated that the introduction of oxygen into MoS_2 nanosheets could lead to more charge carriers and higher intrinsic conductivity of MoS_2 nanosheets.[7e] Moreover, the oxygen incorporation in MoS_2 nanosheets can induce the structure disorder to expose abundant unsaturated sulfur atoms as active sites for HER. As a result, this catalyst exhibited remarkable HER activity with a low onset overpotential of 120 mV and a small Tafel slope of 55 mV decade^{-1}, and the excellent long-term stability.

3) Engineering MoS_2 nanosheet-based composites. To conquer the intrinsic low conductivity and promote the electron-transfer efficiency, various conductive materials were hybridized with MoS_2, such as graphene,[45l,67] CNT,[54,67a] and metals.[7a] All these hybrid structures exhibited enhanced catalytic activity as a result of the synergistic effects between MoS_2 and the conducting matrix materials. Our recent work reported that the solution-processed single-layer MoS_2 nanosheets can be used as templates for the epitaxial growth of well-dispersed 1–3 nm Pt NPs which exposed highly active edge facets (Figure 7 g).[7a] The obtained Pt-MoS_2 hybrid catalyst showed a Tafel slope of approximately 40 mV decade^{-1} and enhanced catalytic activity compared to the commercial Pt-C catalyst on the basis of equal Pt loading (Figure 7 h,i). The excellent performance may be ascribed to the enhanced conductivity and synergetic effects between MoS_2 nanosheets and Pt NPs. The exposed facets of Pt NPs may also contribute to the enhancement of the hydrogen evolution. As another attempt, graphene has been widely used for incorporation with MoS_2 because of its good conductivity and high surface area. The early attempt by Dai and co-workers has demonstrated the excellent catalytic performance of the rGO-MoS_2 hybrid for HER.[45c] Nevertheless, owing to the interlayer attractions, 2D nanostructured materials tend to restack or aggregate in the practical application, which markedly decreases the catalytic performance. Therefore, preparation of 3D electrodes or using 3D conductive materials as support gives great advantages. For example, Liu and co-workers reported the in situ preparation of MoS_2 on mesoporous graphene foams (MoS_2/MGF) for HER.[67b] The mesoporous graphene has a high surface area and interconnected skeleton, which provides more space for the growth of MoS_2 and minimizes the aggregation of MoS_2. Moreover, the incorporation of graphene greatly enhances the electron conductivity of MoS_2/MGF catalyst. The obtained MoS_2/MGF nanocomposite exhibited high catalytic efficiency for HER with low overpotential of 100 mV versus RHE and small Tafel slope of about 42 mV decade^{-1}.

Besides the HER, MoS_2 nanosheet-based nanomaterials are also active for some other electrocatalytic reactions. Very recently, Salehi–Khojin and co-workers demonstrated that the bulk MoS_2 exhibited excellent catalytic activity for reduction of CO_2 in organic electrolyte.[68] Although bulk MoS_2 was used rather than MoS_2 nanosheets, it still provided an example to demonstrate the application of MoS_2 for CO_2 reduction reaction. As another attempt, Wang and coworkers reported that the Pd NP decorated MoS_2 nanosheets could be a good electrocatalyst for methanol oxidation.[42a] The obtained catalyst exhibited higher catalytic activity compared to the commercial Pd/C catalyst. Similarly, by integrating the electron-transport component of graphene, Pt-MoS_2/rGO hybrid materials showed excellent performance for the methanol oxidation and formic acid oxidation.[69] Compare to the commercial Pt/C and Pt-MoS_2 electrodes, Pt-MoS_2/rGO composites exhibited 5.65 and 1.73 times higher electrocatalytic activity for methanol oxidation, respectively. The large surface area of layered materials and enhanced efficiency of charge-transfer in MoS_2/rGO composites could contribute to the improvement of electrocatalytic performance.

4.2. Photocatalysis

Visible light-driven catalysis relies on two properties of the catalyst, that is, the electrocatalytic activity, and the ability to absorb the visible light and separate the electron–hole pair with a certain potential to drive a catalytic reaction.[60b] Bulk MoS_2 itself is not a good candidate as a photocatalyst. However, single- or few-layer MoS_2 nanosheets possess extraordinary photo-induced catalytic ability due to the suitable band gap (i.e. ca. 1.8 eV for single-layer MoS_2). Importantly, the high charge-carrier mobility and large sur-

© 2016 Wiley-VCH Verlag GmbH & Co. KGaA, Weinheim

face-to-volume ratio of MoS_2 nanosheets show great advantages for photo-electrocatalysis. Very recently, our group demonstrated that the hybridization of single-layer TMD (MoS_2 or WS_2) on CdS nanocrystals greatly enhanced the photocatalytic performance of hydrogen evolution (Figure 8a).[44b] The single-layer TMD nanosheets selectively grew on the Cd-rich (0001) surface of wurtzite CdS nanocrystals, offering large percentage of exposed active sites in TMD nanosheets. The hydrogen evolution rate of MoS_2-CdS and WS_2-CdS nanohybrids is 1472 and 1984 $\mu mol\,h^{-1}\,g^{-1}$, which is over 12 and 16 times of that of pure CdS (119 $\mu mol\,h^{-1}\,g^{-1}$), respectively (Figure 8b). Most importantly, the WS_2-CdS nanohybrid showed long-time stability, and 70 % of catalytic activity still remained after 16 h catalytic reaction (Figure 8c). The excellent performance of this TMD-CdS composite may be ascribed to the huge number of active sites in single-layer TMD nanosheets and the inherent p-n heterojunction between TMD and CdS. Figure 8d schematically illustrates the photocatalytic process of the nanohybrids. Upon photo-excitation, CdS NPs can generate the electron–hole pairs, and the electrons can diffuse into the single-layer TMD nanosheet to react with H^+ in water, thus produce the H_2 at the active sites of TMD nanosheets. In another example, Chen and co-workers demonstrated that the 2D porous g-C_3N_4 nanosheets/nitrogen-doped graphene/layered MoS_2 (CNNS/NRGO/MoS_2) ternary nanojunction exhibited photocatalytic activity under visible light.[58a] The g-C_3N_4 nanosheets with large surface area can absorb the visible light, together with the layered MoS_2 to enhance the light absorption and generate more photo-electrons. The ability of charge separation and transfer was improved at the CNNS/MoS_2 interface (sheet to sheet), where the NRGO worked as the electron mediator between the MoS_2 and CNNS in the CNNS/NRGO/MoS_2 composite. Consequently, this hybrid architecture provided a broadening optical window for light harvesting, short diffusion distance for effective charge transport, and large contact area for fast interfacial charge separation. As a result, this CNNS/NRGO/MoS_2 hybrid exhibited enhanced photo-current density and photocatalytic activity for simultaneous oxidation of methylene and reduction of Cr(VI) under the simulated sunlight irradiation.

Traditionally, TiO_2 is widely used in photocatalysis. However, TiO_2 can only absorb the UV light which seriously limits its practical applications. Recently, our group reported the few-layer MoS_2 nanosheet-coated TiO_2 nanobelt (TiO_2@MoS_2) used as a multifunctional photocatalyst for the H_2 evolution and dye degradation.[43c] Compared to the photocatalytic performance of the pure TiO_2 belt, the TiO_2@MoS_2 nanobelt exhibited superior activity. Interestingly, the loading amount of MoS_2 played a key role in determining the catalytic performance. The highest photocatalytic activity of TiO_2@MoS_2 hybrid was obtained when the loading of MoS_2 was 50 wt %, leading to hydrogen production rate of 1.6 $mmol\,h^{-1}\,g^{-1}$. In addition, the TiO_2@MoS_2 hybrid exhibited excellent performance in the absorption and photocatalytic decomposition of organic dyes. The excellent photocatalytic performance was caused by the matched energy band of TiO_2@MoS_2, which favored the charge transfer and suppressed the recombination of photo-generated electrons/holes in TiO_2. In addition, it has also been reported that the titania-based composite containing layered MoS_2/graphene, referred to as MG, and TiO_2 is a high-performance photocatalyst for H_2 production.[43c] Due to the synergetic effect between MoS_2 and graphene sheets, the TiO_2/MoS_2/graphene composite exhibited excellent photocatalytic performance for H_2 evolution with production rate as high as 165.3 $\mu mol\,h^{-1}$ when the content of MG (95 wt % of MoS_2 and 5 wt % of graphene) is 0.5 wt % in the co-catalyst.

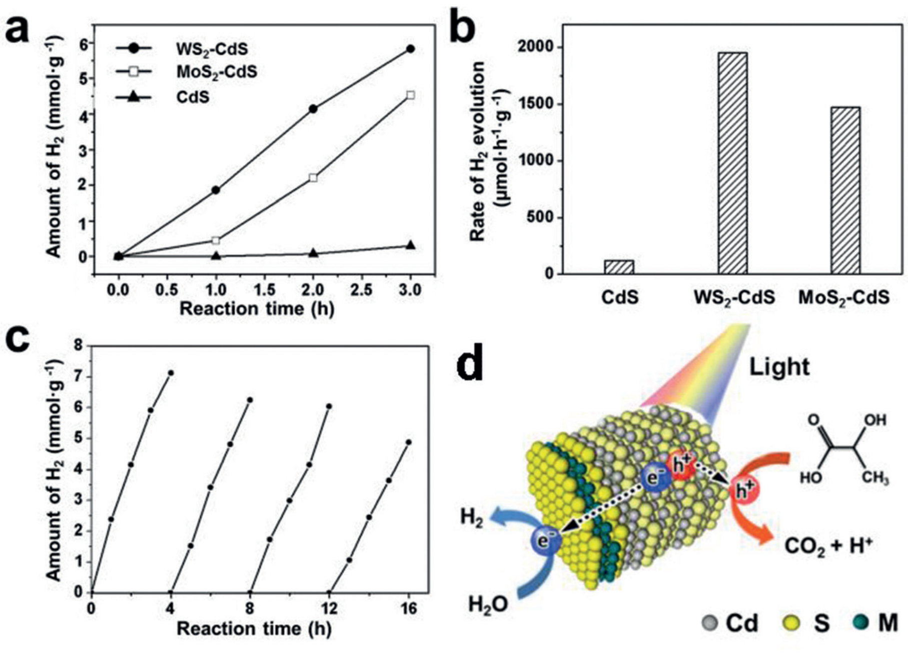

Figure 8. Photocatalytic activity of MS_2–CdS nanohybrids for the hydrogen-evolution reaction. a) Time-dependent photocatalytic H_2 evolution for WS_2–CdS, MoS_2–CdS, and pure CdS. b) The H_2-evolution rate under the visible light irritation for WS_2-CdS, MoS_2-CdS, and pure CdS. c) Cycling test of photocatalytic H_2 evolution for WS_2–CdS. d) Schematic illustration of the photocatalytic process of MS_2–CdS nanohybrid in lactic acid solution. Reproduced with permission from Ref. [44b]. Copyright 2015, John Wiley & Sons, Inc.

4.3. Batteries

The rechargeable lithium-ion battery (LIB) is regarded as one of the most promising power sources for portable electronic devices due to its high energy density, high electromotive force, and great design flexibility.[70] The high surface-to-volume ratio of 2D MoS_2 nanosheets means they offer advantages for LIBs, for example, they enable a tight electrode/electrolyte interaction and a short diffusion path for Li^+ ions and elec-

 © 2016 Wiley-VCH Verlag GmbH & Co. KGaA, Weinheim

trons. Theoretically, 1 mole of MoS_2 is allowed to incorporate 4 mole of lithium (4 electrons transfer reaction per formula), accounting for lithium storage capacity of 670 mAh g^{-1}, which is higher than that of commercial graphite anodes (372 mAh g^{-1}).[7g] However, some disadvantages, such as low conductivity, capacity fading, and poor rate performance of MoS_2 based electrodes, still remain. Therefore, hybridization of MoS_2 nanosheets with complementary materials, such as graphene,[45a,d–g,j,q,71] carbon nanotubes (CNTs),[46d] carbon fibers,[46f,g,55] and metal oxides (e.g., Fe_3O_4, SnO_2 and TiO_2),[43d–f] is a promising and feasible strategy to overcome these weaknesses.

Graphene-based materials are the most promising carbon-based anode matrix for LIBs due to the high electrical conductivity, chemical stability, and good flexibility.[45a,d–g,j,k,q,71] For instance, the anode material composed of layered MoS_2/rGO composite showed high specific capacity of about 1100 mAh g^{-1} at current rate of 100 mA g^{-1}, which is higher than that of both individual components.[45a] The improved performance is ascribed to the synergistic effect between layered MoS_2 and rGO. Specifically, the highly conductive rGO networks not only compensate the relative low conductivity of MoS_2, but also build a 3D architecture to enhance the stability of the electrode during the charge/discharge process, leading to the excellent recycle stability. Following this strategy, several reports for the synthesis of 2D MoS_2-rGO hybrids for LIBs with excellent specific capacities and/or cycling stabilities were presented.[45d–g,j,k,q]

Moreover, the charging and discharging process in LIBs usually causes aggregation of active materials and deterioration of battery performance. Hence, engineering the active materials on substrates as a "skeleton" could be a feasible way to overcome these shortcomings. More specifically, some conductive skeletons can enhance the conductivity of the active materials, and thus boost the performance in LIBs. For example, Lou and co-workers demonstrated that the hybrids of MoS_2 nanosheets on acid-treated CNTs (CNTs@MoS_2) showed excellent performance as anodes for LIBs.[46d] This CNTs@MoS_2-based LIBs showed a reversible capacity of 698 mAh g^{-1} after 60 discharge/charge cycles at a constant current rate of 100 mA g^{-1}, which is higher than that of pure MoS_2 flakes (300 mAh g^{-1}). It was suggested that the large surface area, originating from the 3D hierarchical structure, contributed to the high storage capacity, while the CNTs enhanced the conductivity of the electrode and regulated the volume change during the charge/discharge process. Similarly, MoS_2-nanosheet-decorated carbon-fiber nanocomposites (CNFs@MoS_2) were prepared as anodes for LIBs by Yu and co-workers (Figure 9).[46f] These CNFs@MoS_2 nanofibers exhibited excellent cycling stability with the capacity of 1264 mAh g^{-1} after 50 cycles and high specific capacity of 1489 mAh g^{-1} upon initial discharge (Figure 9a,b). More impressively, the composites showed superior rate performance with the capacity of 864 mAh g^{-1} at a current density of 5 A g^{-1} (Figure 9c,d). Even at 1 A g^{-1}, the CNFs@MoS_2 still demonstrated an excellent high-rate stability after 300 cycles (Figure 9e). It was supposed that the synergistic effect between two components lead to the higher

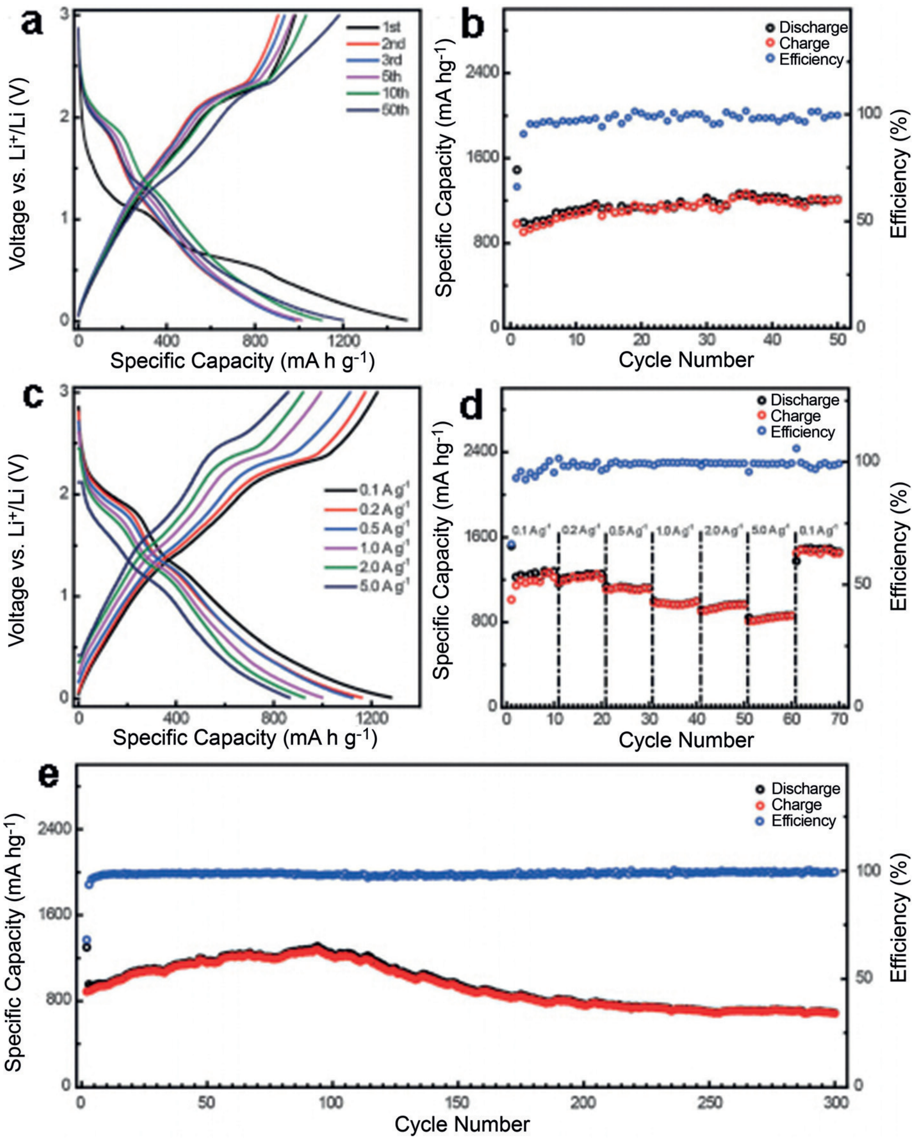

Figure 9. a) Galvanostatic discharge–charge (GDC) profiles and b) cycling performance of CNFs@MoS_2 at 0.1 A g^{-1}. c) GDC profiles and d) cycling performance of CNFs@MoS_2 at different current densities. e) Long-life cycling performance of CNFs@MoS_2 at 1 A g^{-1}. Reproduced with permission from Ref. [46f]. Copyright 2014, John Wiley & Sons, Inc.

capacity. Interestingly, during the charge/discharge process, MoS_2 was continuously oxidized to MoS_3, which also contributed to the increasing capacity upon cycling.

Moreover, hybrid nanostructures based on MoS_2 and metal oxides, such as Fe_3O_4 NPs,[43e] SnO_2,[43f] and TiO_2 nanotubes.[43d] have been extensively studied for LIBs. Generally, metal oxides act as spacers in the composites to prevent the aggregation of MoS_2 nanosheets and make the anode materials accommodate the volume expansion during the charge/discharge process. Therefore, electrodes based on MoS_2–metal oxide composites usually have good cycling stability. For instance, the composite of ultra-small Fe_3O_4-NP-decorated MoS_2 nanosheets used as the anode of LIBs showed superior cyclic stability and rate performances.[43f] Its capacity can reach 1033 $mAh\,g^{-1}$ at current density of 2000 $mA\,g^{-1}$ after 1180 cycles. Even at a high current density of 10000 $mA\,g^{-1}$, the capacity can still remain at 224 $mAh\,g^{-1}$.

Recently, sodium-ion batteries (SIBs) using MoS_2 nanosheet-based hybrid materials have also been reported.[45m,72] For example, Chen and co-workers reported that the graphene-like MoS_2 nanoflowers with an expanded interlayer distance of 0.67 nm were promising as anode materials for rechargeable SIBs with increased Na^+ storage capacity.[73] This kind of MoS_2 electrode showed high discharge capacities of 350 $mAh\,g^{-1}$ at 0.05 $A\,g^{-1}$, 300 $mAh\,g^{-1}$ at 1 $A\,g^{-1}$, and 195 $mAh\,g^{-1}$ at 10 $A\,g^{-1}$. Moreover, Yao and co-workers demonstrated that the interlayer expansion was a general and effective strategy for the development of high-performance electrode materials for SIBs.[74] Typically, the poly(ethylene oxide)-intercalated MoS_2 composite (PEO-MoS_2) was synthesized via a exfoliation–restacking method. The interlayer spacing of the MoS_2 was increased from 0.615 nm to 1.45 nm by insertion of controlled amounts of PEO. Impressively, The bilayer PEO-intercalated MoS_2 composite (PEO_{2L}-MoS_2) with 160% larger interlayer distance exhibited a specific capacity of 225 $mAh\,g^{-1}$ under a current density of 50 $mA\,g^{-1}$, twice as high as that of commercial MoS_2, exhibiting improved rate performance and cycling stability. As another example, Singh and co-workers synthesized a flexible electrode consisting of few-layer MoS_2 and rGO flakes, which showed good performance in SIBs.[45m] During the electrochemical performance test, the composites exhibited a specific capacity of 230 $mAh\,g^{-1}$ and about 99% Coulombic efficiency.

4.4. Biological Applications

The water dispersed MoS_2 nanosheet with large surface area and unique optical properties makes it attractive for various biological applications. Recently, Chou and co-workers demonstrated that the chemically exfoliated MoS_2 nanosheets have a strong absorbance in the near-infrared (NIR) region and could be used as an effective NIR photothermal reagent.[75] Compared to GO, the chemically exfoliated MoS_2 nanosheets display approximately 7.8 times greater NIR absorbance. Moreover, it shows an extinction coefficient of 29.2 $L\,g^{-1}cm^{-1}$ at 800 nm, which is much higher than that of Au nanorods (13.9 $L\,g^{-1}cm^{-1}$) and comparable to rGO (24.6 $L\,g^{-1}cm^{-1}$). Most importantly, the MoS_2 dispersion is heated up rapidly upon irradiation with a wave laser at 800 nm, leading to the possibility of thermal ablation therapy. Because NIR is located in the "optical transmission window" of biological tissues, in which blood and tissue are maximally transparent, MoS_2 nanosheets can be a favorable visualizing tool in biological tissues, as they offer lower photo damage and greater tissue penetration depth. In addition, owing to its high surface-area-to-mass ratio, the exfoliated MoS_2 nanosheets have a high loading capacity of bio-molecular protein, comparable to that of GO. Liu and co-workers demonstrated that the PEG-MoS_2 composite could be a multi-functional drug carrier for integration of photothermal and chemotherapy into a single compound.[41c] Due to the large surface area, the PEG-MoS_2 composites give highly efficient loading of therapeutic molecules, for example, doxorubicin (DOX), 7-ethyl-10-hydroxycamptothecin (SN38), and photodynamic agent chlorine e6 (Ce6). Without noticeable toxicity to cells, DOX loaded MoS_2-PEG composites exhibited excellent synergistic anticancer effect with photothermal and chemotherapy, in both in vitro and in vivo experiments. As shown in Figure 10a, MoS_2-PEG/DOX was used for animal experiments to demonstrate combined photothermal and chemotherapy in vivo. During the irradiation period of NIR light (0.35 $W\,cm^{-2}$, 808 nm), the temperature of tumors injected with MoS_2-PEG or MoS_2-PEG/DOX was significantly increased and higher than the tumors injected with PBS or free DOX (Figure 10b,c), suggesting the efficient photothermal heating effect of MoS_2-based composites. Remarkably, the tumors treated with MoS_2-PEG/DOX under the NIR irradiation were dramatically inhibited, indicating the successful combination of chemotherapy and photothermal therapy (Figure 10d). Significantly, compared to nano-graphene photothermal agents, these PEG-MoS_2 nanosheets require lower usage dose, making them attractive for practical applications. Similarly, Zhao and co-workers demonstrated that chitosan-functionalized MoS_2 nanosheets were capable of simultaneous chemo- and photothermal therapy by NIR stimuli.[41f] The NIR-controlled drug release was observed in the healing of pancreatic cancer. Remarkably, the MoS_2 nanosheets can be simultaneously used as the contrast agent for X-ray computed tomography (CT) imaging, presenting enhanced performance in in vitro imaging compared to the commercial iopromide. The analogues of MoS_2 nanosheets, such as WS_2, were also developed as multifunctional theranostic agents for the in vivo dual-modal CT/photoacoustic imaging-guided photothermal therapy, showing excellent physiological stability.[76]

4.5. Sensors

As a result of their high surface-to-area ratio as well as their unique physical and chemical properties, MoS_2 nanosheets have been used to develop various types of sensors, such as optical sensors,[5a,77] gas sensors,[6a] chemical sensors,[6f,78] and biosensors[6e,79] As an optical sensor, MoS_2 mainly depends on its tunable band gap[80] and fluorescence-quenching ability.[6e] Differently, the remarkable sensitivity of

 © 2016 Wiley-VCH Verlag GmbH & Co. KGaA, Weinheim

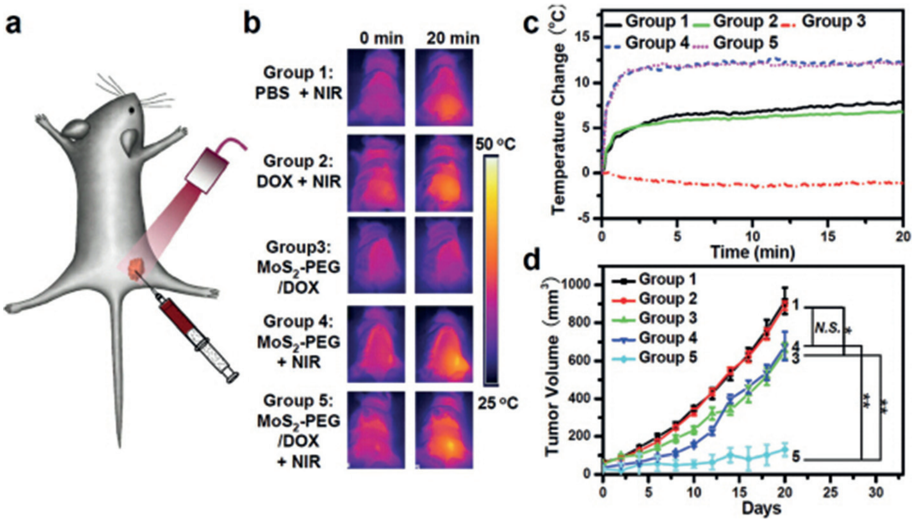

Figure 10. MoS_2–PEG/DOX for in vivo combination therapy. Group 1: PBS + NIR laser; Group 2: DOX + NIR laser; Group 3: MoS_2–PEG/DOX without laser irradiation; Group 4: MoS_2–PEG + NIR laser; Group 5: MoS_2–PEG/DOX + NIR laser. a) Scheme of combination therapy based on the tumor-injected MoS_2–PEG/DOX. b) IR thermal images of 4T1 tumor-bearing mice recorded by an IR camera. The doses DOX and MoS_2–PEG were 0.5 mg kg^{-1} and 0.34 mg kg^{-1}, respectively, in this experiment. Laser irradiation was with a 808 nm NIR laser at a power density of 0.35 W cm^{-2} for 20 min on the tumors. c) Temperature change of tumors monitored by the IR thermal camera in different groups during laser irradiation. d) Tumor volume growth curves of different groups of mice after various treatments (5 mice for each group). Error bars are based on standard errors of the mean (SEM). Reproduced with permission from Ref. [41c]. Copyright 2014, John Wiley & Sons, Inc.

MoS_2-based chemical and gas sensors is mainly ascribed to the charge transfer between the adsorbed molecules and the MoS_2 surface. The adsorption of molecules can dope, or oxidize MoS_2 nanosheets, resulting in the change of electrical resistance of MoS_2. For example, our group has demonstrated the applicability of MoS_2 nanosheet-based thin-film transistors (TFT) for detection of adsorption of NO gases on MoS_2 nanosheets at room temperature.[6a] Because of the p-type MoS_2 channel, the sensing mechanism was ascribed to the p-type doping effect of the electron-withdrawing NO molecules, which changed the electrical resistance of the original MoS_2. The detection limit of the gas sensor was calculated to be 190 ppt which was lower than that of graphene-based TFTs. Later, we developed a flexible TFT array for sensing NO_2 gas by using exfoliated MoS_2 nanosheets as the active channel and rGO film as the drain and source electrodes. Moreover, it was found that if noble metals, such as Pt NPs, decorate the MoS_2 thin films they can greatly enhance the sensitivity of the TFT sensor by about 3 times (Figure 11 a,b).[6b] Except for the gas sensor, we also demonstrated that the electrochemically reduced single-layer MoS_2 nanosheets, which have good conductivity, superior electron-transfer rate, and high electrochemical activity, can be used for detection of glucose and biomolecules.[6d] In addition, the electrochemically reduced single-layer MoS_2 nanosheets exhibited high selectivity towards dopamine in the presence of ascorbic acid and uric acid. Very recently, Jung and co-workers developed a chemresistor sensor for detection of various volatile organic compounds by using ligand-conjugated MoS_2 nanosheets.[6f] Briefly, a thiolated ligand, that is, mercaptoundecanoic acid (MUA), was conjugated on MoS_2 surface through simple solution mixing. Both of the sensors made from the primitive MoS_2 and MUA-conjugated MoS_2 showed high sensitivity (down to 1 ppm) and selectivity toward the representative analytes (toluene, hexane, ethanol, propionaldehyde, propanol, and acetone). However, the sensing behaviors were extremely different, depending on the surface properties of nanosheets and the type of organic compounds. Specifically, the primitive MoS_2 sensor presented a positive response (increase in resistance) for oxygen-functionalized volatile organic compounds (VOCs), while the MUA-conjugated MoS_2 sensor exhibited a negative response (decrease in resistance) for the same analytes (Figure 11 c,d). The low detection limit and tunable response of sensors hold great promise for the early diagnosis of diseases related to the respiratory problems.

In addition to the gas sensing and chemical sensing abilities, our group proposed a simple "mix-and-detect" assay format to detect DNA molecules by using the single-layer MoS_2 nanosheet as the platform and quenching material.[6e] It is suggested that the single-layer MoS_2 nanosheet has a high fluorescence quenching efficiency and different affinities toward the single-stranded DNA (ssDNA) and double-stranded (dsDNA). Typically, the dye-labeled ssDNA probe was decorated on the exfoliated MoS_2 nanosheet via the interaction between nucleobases and the basal plane of MoS_2. The fluorescence of the dye molecules was first quenched by the MoS_2 backbone. However, when the ssDNA hybridized with its complementary target DNA, the interaction between MoS_2 and formed dsDNA molecules became weak, resulting in the larger distance between the dye and MoS_2 surface, thus resulting in the retention of fluorescence of the dye. The fluorescence change was effective for quantitative readout of the DNA molecules. Most importantly, this liquid-phase detection process could be finished within a few minutes, which can be used for automated in situ detection.

4.6. Electronic Devices

Most of the aforementioned applications of MoS_2-based materials rely on the chemical properties and unique structure of MoS_2 nanosheets. In addition, the physical merits of MoS_2, such as tunable band gap, high carrier mobility as well as high on/off current ratio, make it attractive for low-power opto-electronics.[2a,d,3e] In fact, solution-processed MoS_2 nanosheets are not suitable for high-performance electronics, due to the limited lateral size as well as the impurities, such as

 © 2016 Wiley-VCH Verlag GmbH & Co. KGaA, Weinheim

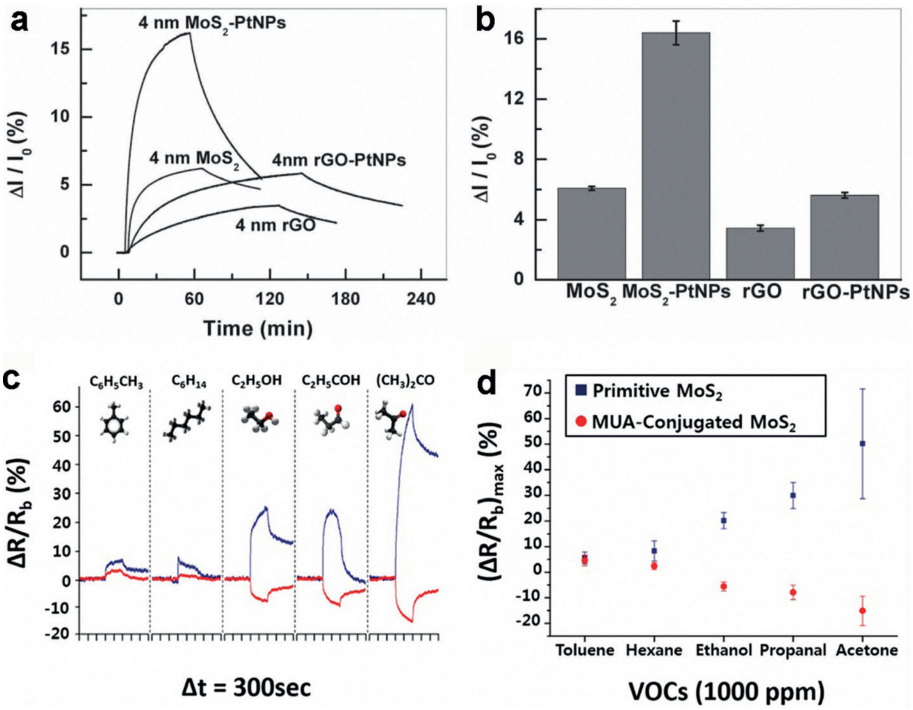

Figure 11. a) Typical current response of TFT sensors on PET upon exposure of 1.2 ppm NO_2 with channels of rGO, rGO-PtNPs, MoS_2, and MoS_2-PtNPs. b) The current change of TFT sensors on PET with channels of rGO, rGO-PtNPs, MoS_2, and MoS_2-PtNPs. Reproduced with permission from Ref. [6b]. Copyright 2012, John Wiley & Sons, Inc. c) The sensor response and d) the maximum amplitude of response within exposure time (10 min) of primitive (blue) and MUA-conjugated (red) MoS_2 sensors for target VOCs (1000 ppm). Target VOCs: toluene, hexane, ethanol, propionaldehyde (propanal), and acetone. Reproduced with permission from Ref. [6f]. Copyright 2014, American Chemical Society.

defects or doping. Despite that, there have been pioneering works to show the feasibility of using solution-processed MoS_2 nanosheets in electronics. For example, Duesberg and co-workers implemented the solution-exfoliated MoS_2 flakes into field effect transistors (FETs).[81] It was found that their electrical properties were comparable with those of mechanically exfoliated samples. Moreover, our group fabricated a single-layer MoS_2-based FET by using electrochemically exfoliated MoS_2 nanosheets (Figure 12a–c). The recorded *I*–*V* curve indicated the p-type behavior of single-layer MoS_2 nanosheet, which is different from the n-type behavior of MoS_2 nanosheets exfoliated by the scotch tape method (Figure 12d).[6a] Recently, MoS_2 nanosheet-based materials have been used for fabrication of memory devices. As a typical example, our group reported that the PVP-coated MoS_2 nanosheets, that is, MoS_2-PVP, can be used as electrically bistable materials for flexible memory devices with the configuration of rGO/MoS_2-PVP/Al.[5d] This device exhibited a nonvolatile rewritable memory behavior with a switching threshold voltage of about 3.5 V and an ON/OFF ratio of approximately 10^2 (Figure 12e). It was suggested that PVP played a crucial role in the electrical transition effect, which was ascribed to the charge trapping and detrapping behavior of MoS_2 in PVP matrix. Inspired by this work, the hybridization of polymers and MoS_2 nanosheets was further developed to enhance the performance of memory devices. Recently, a polymer-assisted self-assembled chiral MoS_2 nanofibers were used as the active layer for fabrication of flexible data-storage devices.[41e] The chiral MoS_2 nanofibers were prepared by self-assembly of MoS_2 nanosheets in highly stirred Pluronic P123 solutions. Impressively, the chiral MoS_2 nanofiber-based memory device presented a typical

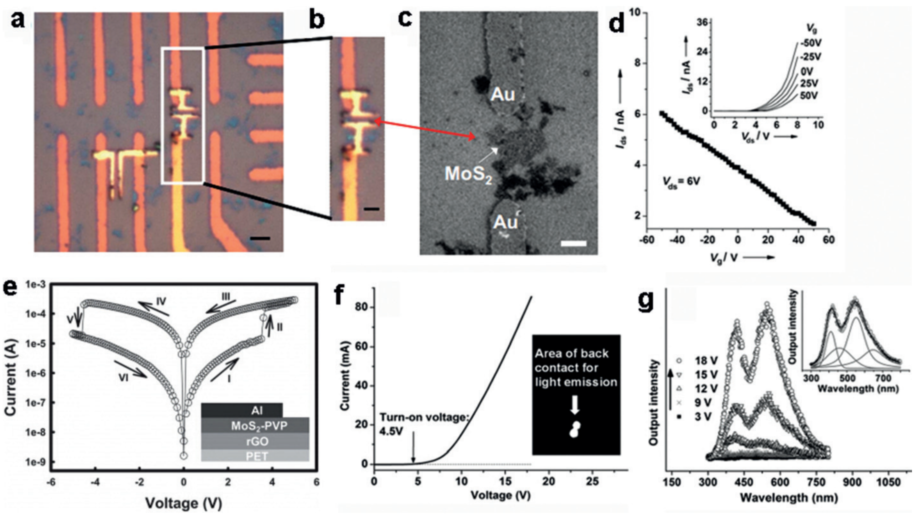

Figure 12. a),b) Optical microscope images of the single-layer MoS_2-based FET device. The scale bars in (a) and (b) represent 2 μm and 1 μm, respectively. c) SEM image of the single-layer MoS_2-based FET device in (b). Scale bar = 1 μm. d) Plot of the drain-to-source current (I_{ds}) versus the gate voltage (V_g) at a drain voltage (V_{ds}) of 6 V. Inset: Plot of the drain-to-source current versus the drain voltage. Reproduced with permission from Ref. [6a]. Copyright 2011, John Wiley & Sons, Inc. e) The *I*–*V* characteristics of the rGO/MoS_2–PVP/Al flexible memory device. Inset: Schematic diagram of the memory device structure. Reproduced with permission from Ref. [5d]. Copyright 2012, John Wiley & Sons, Inc. f) The *I*–*V* curve of an LED with the device configuration of Au/Ti/n-SiC/p-MoS_2–MoO_3/ITO/glass. Inset: photograph of the LED taken at 18 V. g) EL spectra of the LED device biased at different forward voltages. Inset: fitting of sub-bands for the EL spectrum taken at 18 V. Reproduced with permission from Ref. [43h]. Copyright 2014, John Wiley & Sons, Inc.

 © 2016 Wiley-VCH Verlag GmbH & Co. KGaA, Weinheim

nonvolatile flash memory effect with ON/OFF current ratio of 5.5×10^2 as well as excellent reproducibility and good stability. In addition to the polymer-MoS_2 hybrids, Bessonov et al. demonstrated that the MS_2/MO_x (M = Mo, W) heterostructures were also suitable for the fabrication of memory devices when they were used as an active layer and sandwiched between two printed silver electrodes.[43a] The MS_2/MO_x heterostructures were fabricated via deposition of few-layer MS_2 flakes from solution followed by heat-assisted air oxidation. Impressively, the memory device based on the MS_2/MO_x heterostructure exhibited bipolar switching effect with a large and tunable electrical resistance from 10^2 to 10^8 Ω and low programming voltages of 0.1–0.2 V. Most importantly, the bipolar resistive switching effect, with a concurrent capacitive contribution, can be controlled by the ultrathin oxide layer (< 3 nm).

Moreover, recently, our group employed the MoS_2–MoO_3 hybrid for fabrication of light-emitting diodes (LEDs), exhibiting intense multi-wavelengths light emission.[43h] It was evidenced that the MoS_2–MoO_3 composite exhibited p-type conductivity. Therefore, the heterojunction, consisting of p-type MoS_2–MoO_3 (p-MoS_2–MoO_3) film and n-type 4H-SiC (n-SiC) substrate, was used for fabrication of LEDs with configuration of Au/Ti/n-SiC/p-MoS_2–MoO_3/ITO/glass (Figure 12 f,g). The turn-on voltage of this diode was approximately 4.5 V and the electroluminescence (EL) spectra displayed broad emission profiles with four sub-bands located at $\lambda = 411$, 459, 553, and 647 nm.

5. Summary and Outlook

In this Review, the recent progress in preparation, hybridization, and applications of solution-processed MoS_2 nanosheets has been summarized. Specifically, solution-based approaches provide a straightforward way for the scalable production of MoS_2 nanosheets with high yield. Various solution-based methods have been developed for preparation of MoS_2 nanosheets, including the solvent-assisted exfoliation, surfactant/polymer-assisted exfoliation, ion-intercalation and exfoliation, and wet-chemical methods. After being dispersed in solution, MoS_2 nanosheets offer great opportunities for preparation of functional hybrid nanostructures with a variety of materials including organic and biomaterials, MOFs, metals, metal oxides, metal chalcogenides, and carbonaceous materials. Significantly, the MoS_2 nanosheets and their hybrids do show great potentials in various promising applications, such as energy storage and conversion, sensing, electronic and bio-applications.

Although there has been much research in this area, lots of challenges still remain. Currently, the solution-based methods for the preparation of MoS_2 nanosheets have only been used in laboratories and the production quantity of MoS_2 nanosheets is still relatively small, which is unable to meet the requirement for large-scale commercial applications. Therefore, one of the challenges is to develop reliable methods to scale up the production amount of MoS_2 nanosheets, especially the single-layer nanosheets, to meet the criterion for industrial applications. From a hybrid material point of view, it has been reported that the epitaixal growth of Pt NPs on the surface of MoS_2 nanosheets forms Pt-MoS_2 composites, which show higher electrocatalytic activity toward HER due to the exposure of high index facets of Pt NPs induced by the epitaxial effect.[7a] As another example, it has been shown that the edges of MoS_2 are the active sites for HER and the vertically aligned MoS_2 nanosheets with rich edges have better HER catalytic performance.[27,61] However, currently, most of the materials were just simply hybridized with MoS_2 nanosheets by using solution-based methods without much concern as to their hybridization manner, such as the growth orientation, surface exposure and component distribution, or the interaction of each component. Note that these features of a hybrid nanomaterial largely determine its performance in a specific application. Therefore, a big challenge is still the highly controllable construction of hybrid nanomaterials with desired structural features based on solution-processed MoS_2 nanosheets for specific applications.

In the light of current research achievements, there are still many opportunities in this promising field. Recently, lots of 2D lateral and vertical epitaxial MoS_2 nanosheet-based heterojunctions have been prepared by the CVD method and the resultant heterostructures have shown some unique advantages in electronics and photovoltaic devices compared to the pure MoS_2 and artificially stacked heterostructures.[1i,82] Therefore, one of the future directions is to develop effective solution-based methods for the preparation of 2D lateral and vertical epitaxial heterostructures based on MoS_2 nanosheets. One possible way to achieve the epitaxial growth of 2D heterostructures in the solution phase is to further grow another kind of TMD nanosheets (e.g. $MoSe_2$, WS_2, etc.) on the existing MoS_2 nanosheet seeds in solution. Moreover, MoS_2 nanosheets with a high concentration of the metallic 1T phase have shown great potential in electronics, electrocatalysis, and electrochemical supercapacitors.[65,83] The preparation of MoS_2 nanosheets with 100% metallic 1T phase has not been realized yet. Therefore, another promising direction is to prepare pure 1T-phase MoS_2 nanosheets by solution-based methods, which are anticipated to show much enhanced performance in various applications compared to those MoS_2 nanosheets containing 2H phase. The chemical Li-intercalation approach has been demonstrated to be the most effective technique to induce the phase transformation from the 2H to the 1T phase allowing the concentration of metallic 1T phase to reach up to about 80%.[66] Therefore, it may be possible to prepare pure metallic 1T phase MoS_2 nanosheets by finely tuning the experimental conditions, such as reaction time, reaction temperature, and particle size of bulk MoS_2 crystals, or using our recently developed electrochemical lithiation-interclation method,[6a] which has also been shown to produce 1T-phase MoS_2 nanosheets.[7a]

Acknowledgements

This work was supported by MOE under AcRF Tier 2 (ARC 26/13, No. MOE2013-T2-1-034; ARC 19/15, No. MOE2014-T2-2-093) and AcRF Tier 1 (RGT18/13, RG5/13), NTU under Start-Up Grant (M4081296.070.500000) and iFood Research

 © 2016 Wiley-VCH Verlag GmbH & Co. KGaA, Weinheim

Grant (M4081458.070.500000), and Singapore Millennium Foundation in Singapore. This Research is also conducted by NTU-HUJ-BGU Nanomaterials for Energy and Water Management Programme under the Campus for Research Excellence and Technological Enterprise (CREATE), that is supported by the National Research Foundation, Prime Minister's Office, Singapore.

How to cite: *Angew. Chem. Int. Ed.* **2016**, *55*, 8816–8838
Angew. Chem. **2016**, *128*, 8960–8984

[1] a) X. Huang, X. Qi, F. Boey, H. Zhang, *Chem. Soc. Rev.* **2012**, *41*, 666–686; b) C. Tan, Z. Liu, W. Huang, H. Zhang, *Chem. Soc. Rev.* **2015**, *44*, 2615–2628; c) X. Huang, C. Tan, Z. Yin, H. Zhang, *Adv. Mater.* **2014**, *26*, 2185–2204; d) Y. Chen, C. Tan, H. Zhang, L. Wang, *Chem. Soc. Rev.* **2015**, *44*, 2681–2701; e) X. Huang, Z. Yin, S. Wu, X. Qi, Q. He, Q. Zhang, Q. Yan, F. Boey, H. Zhang, *Small* **2011**, *7*, 1876–1902; f) M. Xu, T. Liang, M. Shi, H. Chen, *Chem. Rev.* **2013**, *113*, 3766–3798; g) C. N. R. Rao, H. Matte, U. Maitra, *Angew. Chem. Int. Ed.* **2013**, *52*, 13162–13185; *Angew. Chem.* **2013**, *125*, 13400–13424; h) H. Zhang, *ACS Nano* **2015**, *9*, 9451–9469; i) C. Tan, H. Zhang, *J. Am. Chem. Soc.* **2015**, *137*, 12162–12174.

[2] a) X. Huang, Z. Zeng, H. Zhang, *Chem. Soc. Rev.* **2013**, *42*, 1934–1946; b) C. Tan, H. Zhang, *Chem. Soc. Rev.* **2015**, *44*, 2713–2731; c) M. Chhowalla, Z. Liu, H. Zhang, *Chem. Soc. Rev.* **2015**, *44*, 2584–2586; d) Q. H. Wang, K. Kalantar-Zadeh, A. Kis, J. N. Coleman, M. S. Strano, *Nat. Nanotechnol.* **2012**, *7*, 699–712; e) V. Nicolosi, M. Chhowalla, M. G. Kanatzidis, M. S. Strano, J. N. Coleman, *Science* **2013**, *340*, 1226419; f) M. Chhowalla, H. S. Shin, G. Eda, L.-J. Li, K. P. Loh, H. Zhang, *Nat. Chem.* **2013**, *5*, 263–275.

[3] a) H. Li, J. Wu, Z. Yin, H. Zhang, *Acc. Chem. Res.* **2014**, *47*, 1067–1075; b) H. Li, X. Qi, J. Wu, Z. Zeng, J. Wei, H. Zhang, *ACS Nano* **2013**, *7*, 2842–2849; c) H. Li, G. Lu, Z. Yin, Q. He, H. Li, Q. Zhang, H. Zhang, *Small* **2012**, *8*, 682–686; d) H. Li, J. Wu, X. Huang, G. Lu, J. Yang, X. Lu, Q. Xiong, H. Zhang, *ACS Nano* **2013**, *7*, 10344–10353; e) R. Ganatra, Q. Zhang, *ACS Nano* **2014**, *8*, 4074–4099; f) B. Radisavljevic, A. Radenovic, J. Brivio, V. Giacometti, A. Kis, *Nat. Nanotechnol.* **2011**, *6*, 147–150; g) A. Splendiani, L. Sun, Y. B. Zhang, T. S. Li, J. Kim, C. Y. Chim, G. Galli, F. Wang, *Nano Lett.* **2010**, *10*, 1271–1275; h) G. Eda, H. Yamaguchi, D. Voiry, T. Fujita, M. W. Chen, M. Chhowalla, *Nano Lett.* **2011**, *11*, 5111–5116; i) K. F. Mak, C. Lee, J. Hone, J. Shan, T. F. Heinz, *Phys. Rev. Lett.* **2010**, *105*, 4.

[4] T. Wu, H. Zhang, *Angew. Chem. Int. Ed.* **2015**, *54*, 4432–4434; *Angew. Chem.* **2015**, *127*, 4508–4510.

[5] a) Z. Yin, H. Li, H. Li, L. Jiang, Y. Shi, Y. Sun, G. Lu, Q. Zhang, X. Chen, H. Zhang, *ACS Nano* **2012**, *6*, 74–80; b) Z. Yin, Z. Zeng, J. Liu, Q. He, P. Chen, H. Zhang, *Small* **2013**, *9*, 727–731; c) O. Lopez-Sanchez, D. Lembke, M. Kayci, A. Radenovic, A. Kis, *Nat. Nanotechnol.* **2013**, *8*, 497–501; d) J. Liu, Z. Zeng, X. Cao, G. Lu, L.-H. Wang, Q.-L. Fan, W. Huang, H. Zhang, *Small* **2012**, *8*, 3517–3522.

[6] a) Z. Zeng, Z. Yin, X. Huang, H. Li, Q. He, G. Lu, F. Boey, H. Zhang, *Angew. Chem. Int. Ed.* **2011**, *50*, 11093–11097; *Angew. Chem.* **2011**, *123*, 11289–11293; b) Q. He, Z. Zeng, Z. Yin, H. Li, S. Wu, X. Huang, H. Zhang, *Small* **2012**, *8*, 2994–2999; c) H. Li, Z. Yin, Q. He, H. Li, X. Huang, G. Lu, D. W. H. Fam, A. I. Y. Tok, Q. Zhang, H. Zhang, *Small* **2012**, *8*, 63–67; d) S. X. Wu, Z. Y. Zeng, Q. Y. He, Z. J. Wang, S. J. Wang, Y. P. Du, Z. Y. Yin, X. P. Sun, W. Chen, H. Zhang, *Small* **2012**, *8*, 2264–2270; e) C. Zhu, Z. Zeng, H. Li, F. Li, C. Fan, H. Zhang, *J. Am. Chem. Soc.* **2013**, *135*, 5998–6001; f) J. S. Kim, H. W. Yoo, H. O. Choi, H. T. Jung, *Nano Lett.* **2014**, *14*, 5941–5947.

[7] a) X. Huang, Z. Zeng, S. Bao, M. Wang, X. Qi, Z. Fan, H. Zhang, *Nat. Commun.* **2013**, *4*, 1444; b) X. Cao, Y. Shi, W. Shi, X. Rui, Q. Yan, J. Kong, H. Zhang, *Small* **2013**, *9*, 3433–3438; c) Z. Yin, B. Chen, M. Bosman, X. Cao, J. Chen, B. Zheng, H. Zhang, *Small* **2014**, *10*, 3537–3543; d) Y. F. Yu, S. Y. Huang, Y. P. Li, S. N. Steinmann, W. T. Yang, L. Y. Cao, *Nano Lett.* **2014**, *14*, 553–558; e) J. F. Xie, J. J. Zhang, S. Li, F. Grote, X. D. Zhang, H. Zhang, R. X. Wang, Y. Lei, B. C. Pan, Y. Xie, *J. Am. Chem. Soc.* **2013**, *135*, 17881–17888; f) Y. Yan, B. Xia, Z. Xu, X. Wang, *ACS Catal.* **2014**, *4*, 1693–1705; g) T. Stephenson, Z. Li, B. Olsen, D. Mitlin, *Energy Environ. Sci.* **2014**, *7*, 209–231; h) S. S. Chou, N. Sai, P. Lu, E. N. Coker, S. Liu, K. Artyushkova, T. S. Luk, B. Kaehr, C. J. Brinker, *Nat. Commun.* **2015**, *6*, 8311.

[8] K. S. Novoselov, A. K. Geim, S. V. Morozov, D. Jiang, Y. Zhang, S. V. Dubonos, I. V. Grigorieva, A. A. Firsov, *Science* **2004**, *306*, 666–669.

[9] a) Y. Y. Zhao, X. Luo, H. Li, J. Zhang, P. T. Araujo, C. K. Gan, J. Wu, H. Zhang, S. Y. Quek, M. S. Dresselhaus, Q. H. Xiong, *Nano Lett.* **2013**, *13*, 1007–1015; b) H. L. Zeng, J. F. Dai, W. Yao, D. Xiao, X. D. Cui, *Nat. Nanotechnol.* **2012**, *7*, 490–493; c) H. S. Lee, S. W. Min, Y. G. Chang, M. K. Park, T. Nam, H. Kim, J. H. Kim, S. Ryu, S. Im, *Nano Lett.* **2012**, *12*, 3695–3700.

[10] a) K. K. Liu, W. J. Zhang, Y. H. Lee, Y. C. Lin, M. T. Chang, C. Su, C. S. Chang, H. Li, Y. M. Shi, H. Zhang, C. S. Lai, L. J. Li, *Nano Lett.* **2012**, *12*, 1538–1544; b) Y. J. Zhan, Z. Liu, S. Najmaei, P. M. Ajayan, J. Lou, *Small* **2012**, *8*, 966–971; c) Y. M. Shi, W. Zhou, A. Y. Lu, W. J. Fang, Y. H. Lee, A. L. Hsu, S. M. Kim, K. K. Kim, H. Y. Yang, L. J. Li, J. C. Idrobo, J. Kong, *Nano Lett.* **2012**, *12*, 2784–2791.

[11] a) J. N. Coleman, M. Lotya, A. O'Neill, S. D. Bergin, P. J. King, U. Khan, K. Young, A. Gaucher, S. De, R. J. Smith, I. V. Shvets, S. K. Arora, G. Stanton, H. Y. Kim, K. Lee, G. T. Kim, G. S. Duesberg, T. Hallam, J. J. Boland, J. J. Wang, J. F. Donegan, J. C. Grunlan, G. Moriarty, A. Shmeliov, R. J. Nicholls, J. M. Perkins, E. M. Grieveson, K. Theuwissen, D. W. McComb, P. D. Nellist, V. Nicolosi, *Science* **2011**, *331*, 568–571; b) G. Eda, T. Fujita, H. Yamaguchi, D. Voiry, M. Chen, M. Chhowalla, *ACS Nano* **2012**, *6*, 7311–7317; c) G. Eda, H. Yamaguchi, D. Voiry, T. Fujita, M. W. Chen, M. Chhowalla, *Nano Lett.* **2012**, *12*, 526–526; d) G. Cunningham, M. Lotya, C. S. Cucinotta, S. Sanvito, S. D. Bergin, R. Menzel, M. S. P. Shaffer, J. N. Coleman, *ACS Nano* **2012**, *6*, 3468–3480.

[12] H. Matte, A. Gomathi, A. K. Manna, D. J. Late, R. Datta, S. K. Pati, C. N. R. Rao, *Angew. Chem. Int. Ed.* **2010**, *49*, 4059–4062; *Angew. Chem.* **2010**, *122*, 4153–4156.

[13] a) P.-p. Wang, H. Sun, Y. Ji, W. Li, X. Wang, *Adv. Mater.* **2014**, *26*, 964–969; b) C. Altavilla, M. Sarno, P. Ciambelli, *Chem. Mater.* **2011**, *23*, 3879–3885.

[14] a) A. Ciesielski, P. Samori, *Chem. Soc. Rev.* **2014**, *43*, 381–398; b) Y. Hernandez, V. Nicolosi, M. Lotya, F. M. Blighe, Z. Sun, S. De, I. T. McGovern, B. Holland, M. Byrne, Y. K. Gun'Ko, J. J. Boland, P. Niraj, G. Duesberg, S. Krishnamurthy, R. Goodhue, J. Hutchison, V. Scardaci, A. C. Ferrari, J. N. Coleman, *Nat. Nanotechnol.* **2008**, *3*, 563–568; c) J. Kim, S. Kwon, D.-H. Cho, B. Kang, H. Kwon, Y. Kim, S. O. Park, G. Y. Jung, E. Shin, W.-G. Kim, H. Lee, G. H. Ryu, M. Choi, T. H. Kim, J. Oh, S. Park, S. K. Kwak, S. W. Yoon, D. Byun, Z. Lee, C. Lee, *Nat. Commun.* **2015**, *6*, 8294.

[15] A. O'Neill, U. Khan, J. N. Coleman, *Chem. Mater.* **2012**, *24*, 2414–2421.

[16] H. M. Solomon, B. A. Burgess, G. L. Kennedy, R. E. Staples, *Drug Chem. Toxicol.* **1995**, *18*, 271–293.

[17] a) C. M. Hansen, *Hansen Solubility Parameters: a User's Handbook*, 2nd ed., CRC, Boca Raton, **2007**; b) S. D. Bergin, Z. Sun, D. Rickard, P. V. Streich, J. P. Hamilton, J. N. Coleman, *ACS Nano* **2009**, *3*, 2340–2350.

© 2016 Wiley-VCH Verlag GmbH & Co. KGaA, Weinheim

[18] K.-G. Zhou, N.-N. Mao, H.-X. Wang, Y. Peng, H.-L. Zhang, *Angew. Chem. Int. Ed.* **2011**, *50*, 10839–10842; *Angew. Chem.* **2011**, *123*, 11031–11034.

[19] S. L. Zhang, H. Jung, J. S. Huh, J. B. Yu, W. C. Yang, *J. Nanosci. Nanotechnol.* **2014**, *14*, 8518–8522.

[20] U. Halim, C. R. Zheng, Y. Chen, Z. Lin, S. Jiang, R. Cheng, Y. Huang, X. Duan, *Nat. Commun.* **2013**, *4*, 2213.

[21] L. Dong, S. Lin, L. Yang, J. Zhang, C. Yang, D. Yang, H. Lu, *Chem. Commun.* **2014**, *50*, 15936–15939.

[22] a) R. J. Smith, P. J. King, M. Lotya, C. Wirtz, U. Khan, S. De, A. O'Neill, G. S. Duesberg, J. C. Grunlan, G. Moriarty, J. Chen, J. Wang, A. I. Minett, V. Nicolosi, J. N. Coleman, *Adv. Mater.* **2011**, *23*, 3944–3948; b) B. Mao, Y. Yuan, Y. Shao, B. Yang, Z. Xiao, J. Huang, *J. Comput. Theor. Nanosci.* **2014**, *6*, 685–691; c) L. Guardia, J. I. Paredes, R. Rozada, S. Villar-Rodil, A. Martinez-Alonso, J. M. D. Tascon, *RSC Adv.* **2014**, *4*, 14115–14127.

[23] G. Guan, S. Zhang, S. Liu, Y. Cai, M. Low, C. P. Teng, I. Y. Phang, Y. Cheng, K. L. Duei, B. M. Srinivasan, Y. Zheng, Y.-W. Zhang, M.-Y. Han, *J. Am. Chem. Soc.* **2015**, *137*, 6152–6155.

[24] E. Benavente, M. A. Santa Ana, F. Mendizábal, G. González, *Coord. Chem. Rev.* **2002**, *224*, 87–109.

[25] J. Zheng, H. Zhang, S. Dong, Y. Liu, C. Tai Nai, H. Suk Shin, H. Young Jeong, B. Liu, K. Ping Loh, *Nat. Commun.* **2014**, *5*, 2995.

[26] X. Wang, X. Shen, Z. Wang, R. Yu, L. Chen, *ACS Nano* **2014**, *8*, 11394–11400.

[27] H. Wang, Z. Lu, S. Xu, D. Kong, J. J. Cha, G. Zheng, P.-C. Hsu, K. Yan, D. Bradshaw, F. B. Prinz, Y. Cui, *Proc. Natl. Acad. Sci. USA* **2013**, *110*, 19701–19706.

[28] S. S. Chou, Y.-K. Huang, J. Kim, B. Kaehr, B. M. Foley, P. Lu, C. Dykstra, P. E. Hopkins, C. J. Brinker, J. Huang, V. P. Dravid, *J. Am. Chem. Soc.* **2015**, *137*, 1742–1745.

[29] a) L. Niu, K. Li, H. Zhen, Y.-S. Chui, W. Zhang, F. Yan, Z. Zheng, *Small* **2014**, *10*, 4651–4657; b) G. S. Bang, K. W. Nam, J. Y. Kim, J. Shin, J. W. Choi, S.-Y. Choi, *ACS Appl. Mater. Interfaces* **2014**, *6*, 7084–7089.

[30] Y. G. Yao, L. Tolentino, Z. Z. Yang, X. J. Song, W. Zhang, Y. S. Chen, C. P. Wong, *Adv. Funct. Mater.* **2013**, *23*, 3577–3583.

[31] J.-Y. Wu, M.-N. Lin, L.-D. Wang, T. Zhang, *J. Nanomater.* **2014**, 852735.

[32] Y. Yao, Z. Lin, Z. Li, X. Song, K.-S. Moon, C.-p. Wong, *J. Mater. Chem.* **2012**, *22*, 13494–13499.

[33] E. P. Nguyen, B. Carey, T. Daeneke, J. Z. Ou, K. Latham, S. Zhuiykov, K. Kalantar-Zadeh, *Chem. Mater.* **2015**, *27*, 53–59.

[34] D. Van Thanh, C. C. Pan, C. W. Chu, K. H. Wei, *RSC Adv.* **2014**, *4*, 15586–15589.

[35] N. Liu, P. Kim, J. H. Kim, J. H. Ye, S. Kim, C. J. Lee, *ACS Nano* **2014**, *8*, 6902–6910.

[36] B. L. Cushing, V. L. Kolesnichenko, C. J. O'Connor, *Chem. Rev.* **2004**, *104*, 3893–3946.

[37] J. F. Xie, H. Zhang, S. Li, R. X. Wang, X. Sun, M. Zhou, J. F. Zhou, X. W. Lou, Y. Xie, *Adv. Mater.* **2013**, *25*, 5807–5813.

[38] Y. Lu, X. Yao, J. Yin, G. Peng, P. Cui, X. Xu, *RSC Adv.* **2015**, *5*, 7938–7943.

[39] F. Bonaccorso, A. Lombardo, T. Hasan, Z. Sun, L. Colombo, A. C. Ferrari, *Mater. Today* **2012**, *15*, 564–589.

[40] a) A. A. Green, M. C. Hersam, *Nano Lett.* **2009**, *9*, 4031–4036; b) J. Kang, J.-W. T. Seo, D. Alducin, A. Ponce, M. J. Yacaman, M. C. Hersam, *Nat. Commun.* **2014**, *5*, 5478.

[41] a) D. Voiry, A. Goswami, R. Kappera, C. D. C. E. Silva, D. Kaplan, T. Fujita, M. Chen, T. Asefa, M. Chhowalla, *Nat. Chem.* **2015**, *7*, 45–49; b) S. S. Chou, M. De, J. Kim, S. Byun, C. Dykstra, J. Yu, J. Huang, V. P. Dravid, *J. Am. Chem. Soc.* **2013**, *135*, 4584–4587; c) T. Liu, C. Wang, X. Gu, H. Gong, L. Cheng, X. Shi, L. Feng, B. Sun, Z. Liu, *Adv. Mater.* **2014**, *26*, 3433–3440; d) C. Backes, N. C. Berner, X. Chen, P. Lafargue, P. LaPlace, M. Freeley, G. S. Duesberg, J. N. Coleman, A. R. McDonald, *Angew. Chem. Int. Ed.* **2015**, *54*, 2638–2642; *Angew. Chem.* **2015**, *127*, 2676–2680; e) C. Tan, X. Qi, Z. Liu, F. Zhao, H. Li, X. Huang, L. Shi, B. Zheng, X. Zhang, L. Xie, Z. Tang, W. Huang, H. Zhang, *J. Am. Chem. Soc.* **2015**, *137*, 1565–1571; f) W. Yin, L. Yan, J. Yu, G. Tian, L. Zhou, X. Zheng, X. Zhang, Y. Yong, J. Li, Z. Gu, Y. Zhao, *ACS Nano* **2014**, *8*, 6922–6933; g) S.-K. Kim, J. J. Wie, Q. Mahmood, H. S. Park, *Nanoscale* **2014**, *6*, 7430–7435; h) J. Ge, E.-C. Ou, R.-Q. Yu, X. Chu, *J. Mater. Chem. B* **2014**, *2*, 625–628; i) H. Tang, J. Wang, H. Yin, H. Zhao, D. Wang, Z. Tang, *Adv. Mater.* **2015**, *27*, 1117–1123.

[42] a) L. Yuwen, F. Xu, B. Xue, Z. Luo, Q. Zhang, B. Bao, S. Su, L. Weng, W. Huang, L. Wang, *Nanoscale* **2014**, *6*, 5762–5769; b) L. Pan, Y.-T. Liu, X.-M. Xie, X.-D. Zhu, *Chem. Asian J.* **2014**, *9*, 1519–1524; c) T. S. Sreeprasad, P. Nguyen, N. Kim, V. Berry, *Nano Lett.* **2013**, *13*, 4434–4441; d) H. Sun, J. Chao, X. Zuo, S. Su, X. Liu, L. Yuwen, C. Fan, L. Wang, *RSC Adv.* **2014**, *4*, 27625–27629; e) J. Kim, S. Byun, A. J. Smith, J. Yu, J. Huang, *J. Phys. Chem. Lett.* **2013**, *4*, 1227–1232; f) Y. Shi, J.-K. Huang, L. Jin, Y.-T. Hsu, S. F. Yu, L.-J. Li, H. Y. Yang, *Sci. Rep.* **2013**, *3*, 1839.

[43] a) A. A. Bessonov, M. N. Kirikova, D. I. Petukhov, M. Allen, T. Ryhänen, M. J. A. Bailey, *Nat. Mater.* **2015**, *14*, 199–204; b) J. M. Yun, Y. J. Noh, C. H. Lee, S. I. Na, S. Lee, S. M. Jo, H. I. Joh, D. Y. Kim, *Small* **2014**, *10*, 2319–2324; c) W. J. Zhou, Z. Y. Yin, Y. P. Du, X. Huang, Z. Y. Zeng, Z. X. Fan, H. Liu, J. Y. Wang, H. Zhang, *Small* **2013**, *9*, 140–147; d) X. Xu, Z. Fan, S. Ding, D. Yu, Y. Du, *Nanoscale* **2014**, *6*, 5245–5250; e) Y. Chen, B. Song, X. Tang, L. Lu, J. Xue, *Small* **2014**, *10*, 1536–1543; f) Y. Chen, J. Lu, S. Wen, L. Lu, J. Xue, *J. Mater. Chem. A* **2014**, *2*, 17857–17866; g) Y. P. Huang, Y. E. Miao, L. S. Zhang, W. W. Tjiu, J. S. Pan, T. X. Liu, *Nanoscale* **2014**, *6*, 10673–10679; h) Z. Y. Yin, X. Zhang, Y. Q. Cai, J. Z. Chen, J. I. Wong, Y. Y. Tay, J. W. Chai, J. M. T. Wu, Z. Y. Zeng, B. Zheng, H. Y. Yang, H. Zhang, *Angew. Chem. Int. Ed.* **2014**, *53*, 12560–12565; *Angew. Chem.* **2014**, *126*, 12768–12773; i) P. Qin, G. Fang, W. Ke, F. Cheng, Q. Zheng, J. Wan, H. Lei, X. Zhao, *J. Mater. Chem. A* **2014**, *2*, 2742–2756.

[44] a) J. Schornbaum, B. Winter, S. P. Schießl, F. Gannott, G. Katsukis, D. M. Guldi, E. Spiecker, J. Zaumseil, *Adv. Funct. Mater.* **2014**, *24*, 5798–5806; b) J. Chen, X.-J. Wu, L. Yin, B. Li, X. Hong, Z. Fan, B. Chen, C. Xue, H. Zhang, *Angew. Chem. Int. Ed.* **2015**, *54*, 1210–1214; *Angew. Chem.* **2015**, *127*, 1226–1230; c) A. Anto Jeffery, C. Nethravathi, M. Rajamathi, *J. Phys. Chem. C* **2014**, *118*, 1386–1396; d) F. Withers, H. Yang, L. Britnell, A. P. Rooney, E. Lewis, A. Felten, C. R. Woods, V. Sanchez Romaguera, T. Georgiou, A. Eckmann, Y. J. Kim, S. G. Yeates, S. J. Haigh, A. K. Geim, K. S. Novoselov, C. Casiraghi, *Nano Lett.* **2014**, *14*, 3987–3992.

[45] a) K. Chang, W. Chen, *ACS Nano* **2011**, *5*, 4720–4728; b) Y. Hou, Z. H. Wen, S. M. Cui, X. R. Guo, J. H. Chen, *Adv. Mater.* **2013**, *25*, 6291–6297; c) Y. Li, H. Wang, L. Xie, Y. Liang, G. Hong, H. Dai, *J. Am. Chem. Soc.* **2011**, *133*, 7296–7299; d) L. Ma, G. Huang, W. Chen, Z. Wang, J. Ye, H. Li, D. Chen, J. Y. Lee, *J. Power Sources* **2014**, *264*, 262–271; e) J. Wang, J. Liu, D. Chao, J. Yan, J. Lin, Z. X. Shen, *Adv. Mater.* **2014**, *26*, 7162–7169; f) Y. Liu, Y. Zhao, L. Jiao, J. Chen, *J. Mater. Chem. A* **2014**, *2*, 13109–13115; g) Z. Wang, T. Chen, W. Chen, K. Chang, L. Ma, G. Huang, D. Chen, J. Y. Lee, *J. Mater. Chem. A* **2013**, *1*, 2202–2210; h) B. Zhu, B. Lin, Y. Zhou, P. Sun, Q. Yao, Y. Chen, B. Gao, *J. Mater. Chem. A* **2014**, *2*, 3819–3827; i) Q. J. Xiang, J. G. Yu, M. Jaroniec, *J. Am. Chem. Soc.* **2012**, *134*, 6575–6578; j) Y. Hou, J. Li, Z. Wen, S. Cui, C. Yuan, J. Chen, *Nano Energy* **2014**, *8*, 157–164; k) X. Zhou, Z. Wang, W. Chen, L. Ma, D. Chen, J. Y. Lee, *J. Power Sources* **2014**, *251*, 264–268; l) X. Zheng, J. Xu, K. Yan, H. Wang, Z. Wang, S. Yang, *Chem. Mater.* **2014**, *26*, 2344–2353; m) L. David, R. Bhandavat, G. Singh, *ACS Nano* **2014**, *8*, 1759–1770; n) G. Sun, J. Liu, X. Zhang, X. Wang, H. Li, Y. Yu, W. Huang, H. Zhang, P. Chen, *Angew. Chem. Int. Ed.* **2014**, *53*, 12576–12580; *Angew. Chem.* **2014**, *126*, 12784–12788; o) F. K. Meng, J. T. Li, S. K. Cushing, M. J. Zhi, N. Q. Wu, *J. Am. Chem.*

 © 2016 Wiley-VCH Verlag GmbH & Co. KGaA, Weinheim

Soc. **2013**, *135*, 10286 – 10289; p) K. Chang, Z. W. Mei, T. Wang, Q. Kang, S. X. Ouyang, J. H. Ye, *ACS Nano* **2014**, *8*, 7078 – 7087; q) X. Zhou, L.-J. Wan, Y.-G. Guo, *Chem. Commun.* **2013**, *49*, 1838 – 1840.

[46] a) K. Chang, W. Chen, L. Ma, H. Li, H. Li, F. Huang, Z. Xu, Q. Zhang, J.-Y. Lee, *J. Mater. Chem.* **2011**, *21*, 6251 – 6257; b) C. Yu, Y. Xi, L. Tao, D. Lu, M. Lin, H. Guowei, C. Weixiang, C. Hongzheng, S. Huanxing, X. Mingsheng, *Nanotechnology* **2014**, *25*, 465401; c) S.-Y. Tai, C.-J. Liu, S.-W. Chou, F. S.-S. Chien, J.-Y. Lin, T.-W. Lin, *J. Mater. Chem.* **2012**, *22*, 24753 – 24759; d) S. Ding, J. S. Chen, X. W. Lou, *Chem. Eur. J.* **2011**, *17*, 13142 – 13145; e) Y. Shi, Y. Wang, J. I. Wong, A. Y. S. Tan, C.-L. Hsu, L.-J. Li, Y.-C. Lu, H. Y. Yang, *Sci. Rep.* **2013**, *3*, 2169; f) F. Zhou, S. Xin, H.-W. Liang, L.-T. Song, S.-H. Yu, *Angew. Chem. Int. Ed.* **2014**, *53*, 11552 – 11556; *Angew. Chem.* **2014**, *126*, 11736 – 11740; g) C. Wang, W. Wan, Y. Huang, J. Chen, H. H. Zhou, X. X. Zhang, *Nanoscale* **2014**, *6*, 5351 – 5358.

[47] K. C. Knirsch, N. C. Berner, H. C. Nerl, C. S. Cucinotta, Z. Gholamvand, N. McEvoy, Z. Wang, I. Abramovic, P. Vecera, M. Halik, S. Sanvito, G. S. Duesberg, V. Nicolosi, F. Hauke, A. Hirsch, J. N. Coleman, C. Backes, *ACS Nano* **2015**, *9*, 6018 – 6030.

[48] C. Tan, X. Qi, X. Huang, J. Yang, B. Zheng, Z. An, R. Chen, J. Wei, B. Z. Tang, W. Huang, H. Zhang, *Adv. Mater.* **2014**, *26*, 1735 – 1739.

[49] H. Furukawa, K. E. Cordova, M. O'Keeffe, O. M. Yaghi, *Science* **2013**, *341*, 6149.

[50] a) X. Huang, B. Zheng, Z. Liu, C. Tan, J. Liu, B. Chen, H. Li, J. Chen, X. Zhang, Z. Fan, W. Zhang, Z. Guo, F. Huo, Y. Yang, L.-H. Xie, W. Huang, H. Zhang, *ACS Nano* **2014**, *8*, 8695 – 8701; b) Q. Weng, X. Wang, X. Wang, C. Zhang, X. Jiang, Y. Bando, D. Golberg, *J. Mater. Chem. A* **2015**, *3*, 3097 – 3102; c) K. S. Park, Z. Ni, A. P. Cote, J. Y. Choi, R. D. Huang, F. J. Uribe-Romo, H. K. Chae, M. O'Keeffe, O. M. Yaghi, *Proc. Natl. Acad. Sci. USA* **2006**, *103*, 10186 – 10191; d) G. Lu, J. T. Hupp, *J. Am. Chem. Soc.* **2010**, *132*, 7832 – 7833.

[51] L. Shen, M. Luo, Y. Liu, R. Liang, F. Jing, L. Wu, *Appl. Catal. B* **2015**, *166 – 167*, 445 – 453.

[52] N. Berntsen, T. Gutjahr, L. Loeffler, J. R. Gomm, R. Seshadri, W. Tremel, *Chem. Mater.* **2003**, *15*, 4498 – 4502.

[53] a) G. C. Huang, T. Chen, W. X. Chen, Z. Wang, K. Chang, L. Ma, F. H. Huang, D. Y. Chen, J. Y. Lee, *Small* **2013**, *9*, 3693 – 3703; b) D. Y. Chen, G. Ji, B. Ding, Y. Ma, B. H. Qu, W. X. Chen, J. Y. Lee, *Nanoscale* **2013**, *5*, 7890 – 7896.

[54] Y. Cai, X. Yang, T. Liang, L. Dai, L. Ma, G. W. Huang, W. X. Chen, H. Z. Chen, H. X. Su, M. S. Xu, *Nanotechnology* **2014**, *25*, 465401.

[55] C. Zhao, J. Kong, X. Yao, X. Tang, Y. Dong, S. L. Phua, X. Lu, *ACS Appl. Mater. Interfaces* **2014**, *6*, 6392 – 6398.

[56] a) D. Li, M. B. Muller, S. Gilje, R. B. Kaner, G. G. Wallace, *Nat. Nanotechnol.* **2008**, *3*, 101 – 105; b) S. Guo, S. Dong, *Chem. Soc. Rev.* **2011**, *40*, 2644 – 2672.

[57] F. Meng, J. Li, S. K. Cushing, M. Zhi, N. Wu, *J. Am. Chem. Soc.* **2013**, *135*, 10286 – 10289.

[58] a) Y. Hou, Z. Wen, S. Cui, X. Guo, J. Chen, *Adv. Mater.* **2013**, *25*, 6291 – 6297; b) Q. Xiang, J. Yu, M. Jaroniec, *J. Am. Chem. Soc.* **2012**, *134*, 6575 – 6578.

[59] G. Sun, X. Zhang, R. Lin, J. Yang, H. Zhang, P. Chen, *Angew. Chem. Int. Ed.* **2015**, *54*, 4651 – 4656; *Angew. Chem.* **2015**, *127*, 4734 – 4739.

[60] a) T. F. Jaramillo, K. P. Jorgensen, J. Bonde, J. H. Nielsen, S. Horch, I. Chorkendorff, *Science* **2007**, *317*, 100 – 102; b) A. B. Laursen, S. Kegnaes, S. Dahl, I. Chorkendorff, *Energy Environ. Sci.* **2012**, *5*, 5577 – 5591.

[61] J. Kibsgaard, Z. Chen, B. N. Reinecke, T. F. Jaramillo, *Nat. Mater.* **2012**, *11*, 963 – 969.

[62] S. Xu, D. Li, P. Wu, *Adv. Funct. Mater.* **2015**, *25*, 1127 – 1136.

[63] M.-R. Gao, M. K. Y. Chan, Y. Sun, *Nat. Commun.* **2015**, *6*, 7493.

[64] H. Tributsch, *Ber. Bunsen-Ges.* **1977**, *81*, 361 – 369.

[65] a) Q. Ding, F. Meng, C. R. English, M. Caban-Acevedo, M. J. Shearer, D. Liang, A. S. Daniel, R. J. Hamers, S. Jin, *J. Am. Chem. Soc.* **2014**, *136*, 8504 – 8507; b) M. A. Lukowski, A. S. Daniel, F. Meng, A. Forticaux, L. Li, S. Jin, *J. Am. Chem. Soc.* **2013**, *135*, 10274 – 10277.

[66] D. Voiry, M. Salehi, R. Silva, T. Fujita, M. W. Chen, T. Asefa, V. B. Shenoy, G. Eda, M. Chhowalla, *Nano Lett.* **2013**, *13*, 6222 – 6227.

[67] a) D. H. Youn, S. Han, J. Y. Kim, J. Y. Kim, H. Park, S. H. Choi, J. S. Lee, *ACS Nano* **2014**, *8*, 5164 – 5173; b) L. Liao, J. Zhu, X. Bian, L. Zhu, M. D. Scanlon, H. H. Girault, B. Liu, *Adv. Funct. Mater.* **2013**, *23*, 5326 – 5333.

[68] M. Asadi, B. Kumar, A. Behranginia, B. A. Rosen, A. Baskin, N. Repnin, D. Pisasale, P. Phillips, W. Zhu, R. Haasch, R. F. Klie, P. Král, J. Abiade, A. Salehi-Khojin, *Nat. Commun.* **2014**, *5*, 4470.

[69] C. Zhai, M. Zhu, D. Bin, F. Ren, C. Wang, P. Yang, Y. Du, *J. Power Sources* **2015**, *275*, 483 – 488.

[70] a) J. M. Tarascon, M. Armand, *Nature* **2001**, *414*, 359 – 367; b) P. G. Bruce, B. Scrosati, J.-M. Tarascon, *Angew. Chem. Int. Ed.* **2008**, *47*, 2930 – 2946; *Angew. Chem.* **2008**, *120*, 2972 – 2989; c) H. Li, Z. Wang, L. Chen, X. Huang, *Adv. Mater.* **2009**, *21*, 4593 – 4607.

[71] S. Han, Y. Zhao, Y. Tang, F. Tan, Y. Huang, X. Feng, D. Wu, *Carbon* **2015**, *81*, 203 – 209.

[72] Y.-X. Wang, S.-L. Chou, D. Wexler, H.-K. Liu, S.-X. Dou, *Chem. Eur. J.* **2014**, *20*, 9607 – 9612.

[73] Z. Hu, L. Wang, K. Zhang, J. Wang, F. Cheng, Z. Tao, J. Chen, *Angew. Chem. Int. Ed.* **2014**, *53*, 12794 – 12798; *Angew. Chem.* **2014**, *126*, 13008 – 13012.

[74] Y. Li, Y. Liang, F. C. Robles Hernandez, H. Deog Yoo, Q. An, Y. Yao, *Nano Energy* **2015**, *15*, 453 – 461.

[75] S. S. Chou, B. Kaehr, J. Kim, B. M. Foley, M. De, P. E. Hopkins, J. Huang, C. J. Brinker, V. P. Dravid, *Angew. Chem. Int. Ed.* **2013**, *52*, 4160 – 4164; *Angew. Chem.* **2013**, *125*, 4254 – 4258.

[76] L. Cheng, J. J. Liu, X. Gu, H. Gong, X. Z. Shi, T. Liu, C. Wang, X. Y. Wang, G. Liu, H. Y. Xing, W. B. Bu, B. Q. Sun, Z. Liu, *Adv. Mater.* **2014**, *26*, 1886 – 1893.

[77] Y. Tan, R. He, C. Cheng, D. Wang, Y. Chen, F. Chen, *Sci. Rep.* **2014**, *4*, 7523.

[78] F. K. Perkins, A. L. Friedman, E. Cobas, P. M. Campbell, G. G. Jernigan, B. T. Jonker, *Nano Lett.* **2013**, *13*, 668 – 673.

[79] J. Lee, P. Dak, Y. Lee, H. Park, W. Choi, M. A. Alam, S. Kim, *Sci. Rep.* **2014**, *4*, 7354.

[80] S. Balendhran, S. Walia, H. Nili, J. Z. Ou, S. Zhuiykov, R. B. Kaner, S. Sriram, M. Bhaskaran, K. Kalantar-zadeh, *Adv. Funct. Mater.* **2013**, *23*, 3952 – 3970.

[81] K. Lee, H. Y. Kim, M. Lotya, J. N. Coleman, G. T. Kim, G. S. Duesberg, *Adv. Mater.* **2011**, *23*, 4178 – 4182.

[82] a) M.-Y. Li, Y. Shi, C.-C. Cheng, L.-S. Lu, Y.-C. Lin, H.-L. Tang, M.-L. Tsai, C.-W. Chu, K.-H. Wei, J.-H. He, W.-H. Chang, K. Suenaga, L.-J. Li, *Science* **2015**, *349*, 524 – 528; b) Y. Gong, J. Lin, X. Wang, G. Shi, S. Lei, Z. Lin, X. Zou, G. Ye, R. Vajtai, B. I. Yakobson, H. Terrones, M. Terrones, B. K. Tay, J. Lou, S. T. Pantelides, Z. Liu, W. Zhou, P. M. Ajayan, *Nat. Mater.* **2014**, *13*, 1135 – 1142; c) G. S. Duesberg, *Nat. Mater.* **2014**, *13*, 1075 – 1076.

[83] a) D. Voiry, A. Mohite, M. Chhowalla, *Chem. Soc. Rev.* **2015**, *44*, 2702 – 2712; b) M. Acerce, D. Voiry, M. Chhowalla, *Nat. Nanotechnol.* **2015**, *10*, 313 – 318.

Received: October 24, 2015
Published online: June 22, 2016

 © 2016 Wiley-VCH Verlag GmbH & Co. KGaA, Weinheim